



Complex fault patterns, transtension and structural segmentation of the Lofoten Ridge, Norwegian margin: Using digital mapping to link onshore and offshore geology

Robert W. Wilson,¹ Kenneth J. W. McCaffrey,¹ Robert E. Holdsworth,¹ Jonathan Imber,¹ Richard R. Jones,^{2,3} Alastair I. F. Welbon,⁴ and David Roberts⁵

Received 23 August 2005; revised 27 April 2006; accepted 30 May 2006; published 26 August 2006.

[1] An integrated onshore-offshore study involving regional to outcrop-scale fault analysis is used to develop a self-consistent structural model for transtension along the Lofoten Ridge. The Lofoten-Vesterålen archipelago (LVA) is a segmented basement high showing distinct lateral variations in trend, deformational style, and structural complexity. This study investigates whether segmentation can be linked to differences in the obliquity of preexisting structures relative to plate movement vectors. Regional analysis of fault lineament patterns using Geographic Information Systems (GIS) reveals that the LVA can be subdivided into a series of distinct lineament domains. These domains are closely coincident with changes in ridge trend and variations in structure within offshore models derived from seismic reflection studies. Digital field mapping and spatial analysis of faulting in the north Lofoten reveal that multimodal faulting is dominated by transtensional dip-slip and oblique-slip movements which are comparable to analogue models where the ridge axis is 30° oblique to regional extension. The overall change in fault orientation, fault geometry, and deformation style are consistent with models for transtension where the ridge-bounding structure becomes increasingly oblique to regional extension. Previously identified transfer zones simply reflect segment domain boundaries and are not reactivating basement structures. This model is a possible analogue for other orthogonal and oblique rift structures on the Norwegian and other margins. **Citation:** Wilson, R. W., K. J. W. McCaffrey, R. E. Holdsworth, J. Imber, R. R. Jones, A. I. F. Welbon, and D. Roberts (2006), Complex fault patterns, transtension and structural segmentation of the Lofoten Ridge, Norwegian margin: Using digital mapping to link onshore and

offshore geology, *Tectonics*, 25, TC4018, doi:10.1029/2005TC001895.

1. Introduction

[2] Most passive margins are segmented along strike, giving rise to discrete zones characterized by constancy in structural style [e.g., *Francheteau and Le Pichon*, 1972; *Doré et al.*, 1997; *Clemson et al.*, 1997; *Song et al.*, 2001]. This segmentation is also seen in continental rifts that are the precursor to these passive margins [e.g., *Rosendahl*, 1987; *Morley et al.*, 1990]. The boundaries between margin/rift segments are generally believed to exhibit a variety of structural styles ranging from transfer faults [*Gibbs*, 1984] and accommodation zones [*Bosworth et al.*, 1986] to transform faults. The origins of this segmentation and segment boundary zones are often attributed to the influence of basement structure [e.g., *Davison*, 1997; *Clemson et al.*, 1997]. One possibility is that such segmentation reflects along-strike changes in the orientation of preexisting structures in the underlying continental basement. A corollary of this model is that if such preexisting structures undergo reactivation then they will often be significantly oblique to the direction of regional extension. This leads to the development of zones of oblique extension or transtension on what would otherwise be a simple extensional margin [*Dewey*, 2002; *Morley et al.*, 2004].

[3] Transtension may be described as oblique extension which combines coaxial orthogonal extension and noncoaxial deformation zone parallel shear [*Sanderson and Marchini*, 1984; *Dewey*, 2002]. Transtensional strain will occur when bulk displacement is at an oblique angle α to the deformation zone boundary faults (Figure 1a). Pure shear coaxial extension ($\alpha = 90^\circ$) and noncoaxial wrench simple shear ($\alpha = 0^\circ$) represent the end-member strain states for transtension, both of which lead to plane strain (two-dimensional) deformation. Transtension ($0^\circ < \alpha < 90^\circ$) on the other hand results in noncoaxial three-dimensional (3-D) strain [*De Paola et al.*, 2005a]. Transtensional strains are characterized by complex relationships between finite and infinitesimal strain axes that critically depend on the angle α (Figure 1). In extension-dominated transtension ($20^\circ < \alpha < 90^\circ$) the axes of infinitesimal (z) and finite shortening (Z) should always be coincident and vertical, which is comparable to the case of orthogonal extension ($\alpha = 90^\circ$) (Figures 1b) [*McCoss*, 1986; *Smith and Durney*, 1992; *De Paola et al.*, 2005a]. However, at low angles of divergence ($\alpha < 20^\circ$), the infinitesimal axis z is

¹Reactivation Research Group, Department of Earth Sciences, University of Durham, Durham, UK.

²Geospatial Research Ltd., Department of Earth Sciences, University of Durham, Durham, UK.

³e-Science Research Institute, University of Durham, Durham, UK.

⁴Statoil ASA, Stavanger, Norway.

⁵Geological Survey of Norway, Trondheim, Norway.

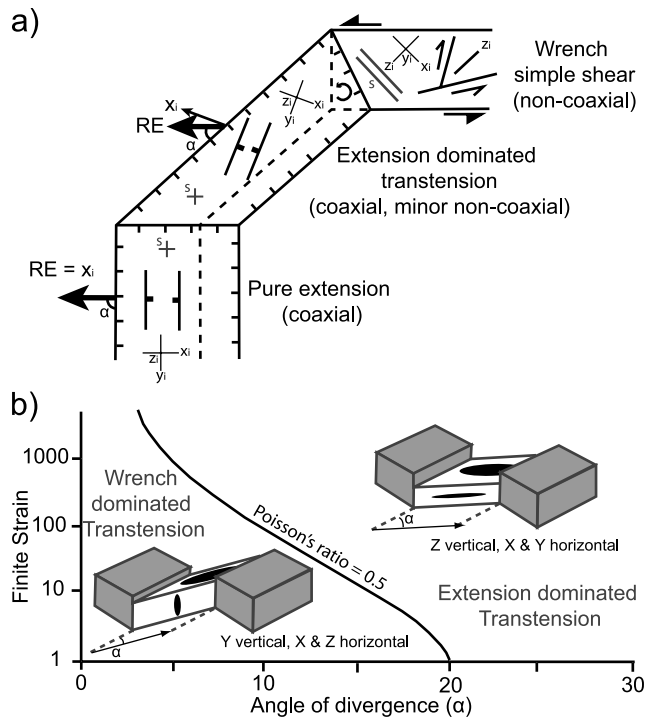


Figure 1. (a) Schematic plan view diagram showing an example of transtension (in this example extension-dominated transtension) in an increasingly oblique margin [after Dewey, 2002]. RE, regional extension direction. (b) Cartoon graph showing horizontal finite strain versus angle of divergence, α . Solid curved line highlights the angle α_{crit} which marks the transition from wrench-dominated to extension-dominated transtension for materials with a Poisson's ratio of 0.5 (modified from Teyssier and Tikoff [1999]).

horizontal, with the finite axis (Z) eventually swapping orientation with the vertical intermediate finite axis Y with increasing amounts of finite strain (“wrench-dominated transtension”; Figure 1b). It is not surprising, therefore, that both field- and laboratory-based studies of deformation styles in oblique and transtensional settings have shown that these zones exhibit more complex fault patterns than those traditionally associated with orthogonal rifting [e.g., Withjack and Jamison, 1986; Schreurs and Colletta, 1998; Clifton et al., 2000; McClay et al., 2002; Dewey, 2002; De Paola et al., 2005a]. Furthermore, the presence of preexisting structures lying at an oblique angle to imposed opening vectors may commonly lead to the partitioning of oblique rifting into contemporaneous domains of wrench- and extension-dominated transtension [Titus et al., 2002; Oldow, 2003; De Paola et al., 2005b].

[4] The Norwegian continental margin is a well documented example of a segmented passive margin [Doré et al., 1997; Tsikalas et al., 2001; Olesen et al., 2002; Mosar, 2003]. This segmentation is generally defined by the presence of a series of approximately NW-SE trending cross-

margin accommodation/transfer zones (Figures 2a and 2b) [Blystad et al., 1995; Olesen et al., 1997, 2002; Brekke, 2000; Tsikalas et al., 2001]. These transfer zones are believed to reflect major basement structures at depth [Strömberg, 1976; Mjelde et al., 2003]. This appears to be true for the largest transfer zones (e.g., Jan Mayen, Bivrost, Senja fracture zones), which we term here first-order transfer zones. However, others are simply inferred across areas of changing fault trend, fault polarity or basin geometry (e.g., Mosken and Jannegga transfer zones) [Tsikalas et al., 2001], and in many cases no attributable basement structure is observed. These we term second-order transfer zones, and they are more comparable to accommodation zones and twist zones [Colletta et al., 1988; Peacock et al., 2000].

[5] In this paper, we shall use integrated regional to outcrop-scale onshore and offshore studies to investigate the variations in fault pattern and structural style across a zone of increasing obliquity relative to the regional extension vector. Furthermore, we investigate the hypothesis that it is the orientation of individual ridge/margin segments, and their bounding faults, relative to regional extension that controls fault complexity and the development of second-order transfer structures.

[6] The Lofoten Ridge (Figure 2b) is a basement ridge showing distinct lateral variations in trend, and provides a good opportunity to compare fault architectures found in crystalline basement onshore [Tveten and Zwaan, 1993; Løseth and Tveten, 1996; Olesen et al., 1997; Klein and Steltenpohl, 1999; Steltenpohl et al., 2004], with those developed in sedimentary basins offshore [Mokhtari and Pegrum, 1992; Løseth and Tveten, 1996; Tsikalas et al., 2001]. The Lofoten Ridge has been strongly affected by tectonic activity during the Late Mesozoic extension prior to the separation of Norway and Greenland and, given its curved geometry, is an ideal location to look for evidence of basement-influenced oblique extension. The area is also an excellent analogue for offshore basement fault blocks beneath the Norwegian and other passive margins.

[7] In the present study, we apply new digital mapping workflows [Jones et al., 2004; Wilson et al., 2005; McCaffrey et al., 2005] to construct a structural database for both onshore and offshore structures on the Lofoten-Vesterålen archipelago (LVA; Figure 2c). All data are stored digitally in a Geographic Information System (GIS) database that facilitates the interpretation of multiple/integrated data sets (e.g., seismic data, remote sensing, field mapping [Jones et al., 2004; Piazzolo et al., 2004]). It also provides an ability to analyze structures spatially across a wide range of scales.

2. Regional Setting

2.1. Lofoten-Vesterålen Margin

[8] Past studies have shown that the Norwegian continental margin can be divided into a series of segments (Møre, Vøring, Lofoten-Vesterålen, and Western Barents Sea margins; Figure 2) [Talwani and Eldholm, 1977; Olesen et al., 1997; Doré et al., 1999; Brekke, 2000; Mosar, 2003]. The Lofoten-Vesterålen Margin segment lies between the

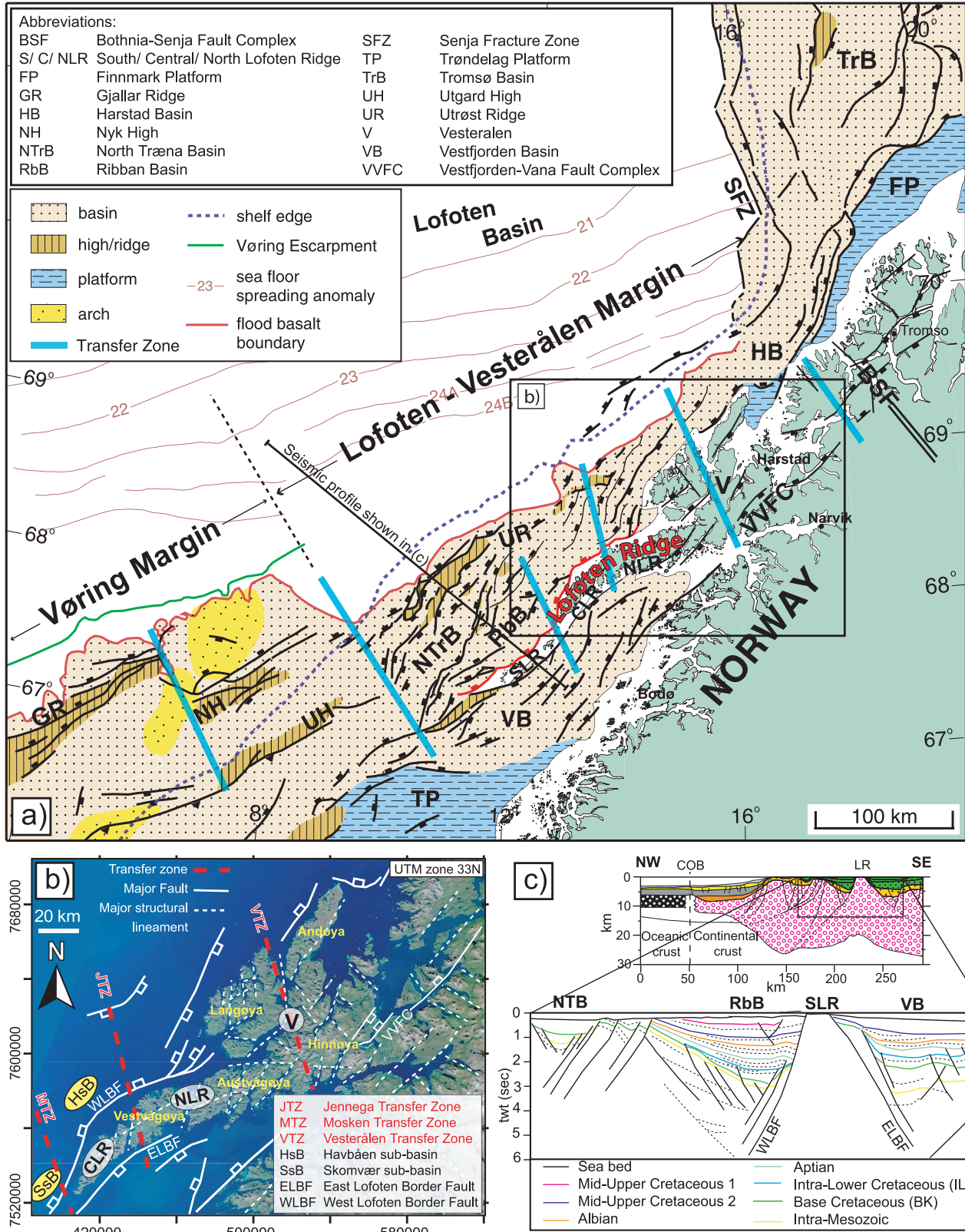


Figure 2. (a) Tectonomagmatic map of the Lofoten-Vesterålen margin (modified from *Tsikalas et al. [2001]*). (b) Landsat image of the Lofoten-Vesterålen archipelago. The transfer zones proposed in past studies are highlighted in red [*Olesen et al., 1997, 2002; Tsikalas et al., 2001*]. (c) Simplified cross sections across the Lofoten-Vesterålen margin and south Lofoten Ridge (modified from *Tsikalas et al. [2001]*).

Bivrost and Senja fracture zones (Figure 2) [Eldholm *et al.*, 1979; Tsikalas *et al.*, 2001]. Compared to its neighboring margin segments, the Lofoten-Vesterålen Margin has a relatively narrow continental shelf and steep slope. Seismic and geophysical studies in this segment show a rift complex of margin-parallel basement ridges and shallow Mesozoic basins [Mokhtari and Pegrum, 1992; Løseth and Tveten, 1996; Olesen *et al.*, 1997, 2002; Tsikalas *et al.*, 2001]. Tsikalas *et al.* [2001] further subdivide the margin into a series of intramargin segments based on changes in fault polarity and intensity. These intramargin segments are thought to be separated by transfer zones (Jannegga, Vesterålen; Figure 2a), also identified by Olesen *et al.* [1997, 2002].

[9] The Norwegian margin has a prolonged Paleozoic to Cenozoic history of intermittent extension and basin formation dating from the Devonian postorogenic (i.e., post-Scandian) collapse of the Caledonide mountain belt [Fossen and Dunlap, 1998; Doré *et al.*, 1999; Fossen, 2000]. Regional extension episodes have been documented in the Devonian-Carboniferous, Permian, through the Late Jurassic to Early Cretaceous, and in Late Cretaceous to Early Cenozoic times [Blystad *et al.*, 1995; Lundin and Doré, 1997; Brekke, 2000]. The last extensional event is considered to have culminated in continental breakup and massive igneous activity at the Paleocene-Eocene transition, ~55 Ma [Eldholm *et al.*, 1989; Skogseid *et al.*, 1992, 2000; Eide, 2002; Ren *et al.*, 2003].

[10] Late Jurassic–Early Cretaceous rifting is the dominant tectonic episode that gave rise to the prominent NE-SW trending faults on the margin [Blystad *et al.*, 1995; Doré *et al.*, 1999; Brekke, 2000; Tsikalas *et al.*, 2001; Mosar, 2003]. There are two dominant NE-SW oriented ridges on the Lofoten-Vesterålen Margin: the Lofoten Ridge and the Utrøst Ridge (Figures 2a and 2c). Extensive synrift thickening of Lower Cretaceous sequences is apparent along faults bordering the western flank of the Lofoten Ridge, indicating that tectonism was active until about Hauterivian time, ~130 Ma [Doré *et al.*, 1999; Tsikalas *et al.*, 2001].

2.2. Lofoten-Vesterålen Archipelago

[11] The inner Lofoten-Vesterålen margin is dominated by the Lofoten Ridge, which can be split into three sections (north, central, and south) showing variations in trend (Figure 2a). With the exception of a few small islands (e.g., Røst and Værøy), the south Lofoten Ridge lies below sea level (Figure 2a), whereas the central and north Lofoten Ridge make up part of the Lofoten-Vesterålen archipelago (LVA) (Figure 2b). Collectively, the ridge marks a prominent NE-SW trending horst, bound on both sides by deep sedimentary basins (Vestfjorden and Ribban basins) [Mokhtari and Pegrum, 1992; Blystad *et al.*, 1995; Løseth and Tveten, 1996]. The archipelago is composed mainly of high-grade metamorphic Precambrian rocks [Griffin *et al.*, 1978] which have undergone a multistage exhumation history [Griffin *et al.*, 1978; Hendriks, 2003]. The exposed rocks are mainly migmatitic gneisses that were metamorphosed to amphibolite and granulite facies, and extensively

intruded by mangeritic and charnockitic plutons [Griffin *et al.*, 1978; Corfu, 2004a]. U-Pb dating of these plutons suggest that the main phase of emplacement was between 1800 and 1790 Ma [Corfu, 2004a] and make up the bulk of the rocks exposed in north Lofoten (i.e., on Austvågøya and Vestvågøya) [Tveten, 1978; Corfu, 2004a]. Basement fabrics within these rocks are somewhat variable, both in trend and intensity, along the ridge [Tveten, 1978]. Unlike other exposures of the Western Gneiss Region, the Caledonian fabrics are only weakly developed in these basement rocks of the LVA [Griffin *et al.*, 1978; Tull *et al.*, 1985; Steltenpohl *et al.*, 2004]. This has been attributed to the lack of fluids in the dry granulite facies basement in the area [Bartley, 1982; Olesen *et al.*, 1997]. Separating these Precambrian basement terranes from the Caledonian nappe sequences to the east are a series of steeply dipping brittle-ductile to cataclastic faults called the Vestfjorden-Vanna fault complex (Figure 2) [Andresen and Forslund, 1987; Olesen *et al.*, 1997]. This fault zone has been attributed to Late Jurassic–Early Cretaceous movements [Andresen and Forslund, 1987], although older Permian movements have also been suggested [Olesen *et al.*, 1997; Steltenpohl *et al.*, 2004].

[12] The only onshore exposures of nonbasement rocks can be found on Andøya [Dalland, 1981], where Jurassic and Lower Cretaceous sediments outcrop. Similar age sediments have also been documented from within fjords on Vesterålen [e.g., Davidsen *et al.*, 2001].

[13] A large fault defines the western flank of the Lofoten Ridge (the West Lofoten Border Fault, WLBF [Løseth and Tveten, 1996]), and also forms the major bounding fault to the Ribban Basin offshore (Figure 2). This basin is subdivided into the Skomvær and Havbåen subbasins (Figure 2b) [Mokhtari and Pegrum, 1992; Olesen *et al.*, 1997; Tsikalas *et al.*, 2001]. In places, the WLBF has a cumulative throw to the west or NW in excess of 3 km [Tsikalas *et al.*, 2001]. Traced northward, the WLBF changes orientation from a NNE-SSW trend to NE-SW/ENE-WSW trend between Moskenesøya and Vestvågøya (Figure 2b), and this is reflected in the overall trend of the Lofoten Ridge. This change is coincident with an apparent change in fault polarity within the Ribban Basin from dominantly NW dipping in the south to dominantly SE dipping in the north [Tsikalas *et al.*, 2001]. It also coincides with a decrease in throw on the Eastern Lofoten Border Fault (ELBF; Figure 2b) northward. These observations led both Tsikalas *et al.* [2001] and Olesen *et al.* [2002] to infer a transfer zone through the area (Figures 2a and 2b); however, the exact trend and location are still debated.

[14] Another major transfer zone has been inferred to run through Vesterålen [Olesen *et al.*, 1997, 2002; Tsikalas *et al.*, 2001]. However, apart from a few discrete NW-SE trending strike-slip faults running across Vesterålen that may be associated with this transfer structure, no major transverse fault is apparent. The transfer zone is instead characterized by an apparent regional barrier to the propagation of NE-SW faults [Olesen *et al.*, 1997]. This region has been described as a “twist zone” by Olesen *et al.* [1997, 2002], and is comparable to the “transfer zones” or “ac-

commodation zones” described by *Peacock et al.* [2000]. Also spatially coincident with this inferred transfer zone on Vesterålen is a steep magnetic gradient oriented NNW-SSE with a positive anomaly to the west and a negative anomaly to the east. This boundary has been attributed to the prograde metamorphic transition from amphibolite-facies migmatites in the east to granulite-facies rocks in the west [*Griffin et al.*, 1978; *Olesen et al.*, 1991]. However, *Corfu* [2004b] has proposed alternatively that this gradient marks a major Caledonian tectonic boundary on Vesterålen.

[15] All transfer zones that have been inferred in the region (Figure 2) are based on changes in fault polarity and sediment thickness offshore [*Tsikalas et al.*, 2001], and variation in crustal structure onshore [*Løseth and Tveten*, 1996; *Olesen et al.*, 1997, 2002]. All follow a preferred NNW-SSE to NW-SE orientation, which may be linked to the influence of Proterozoic shear zones within basement (e.g., the Bothnian-Senja Fault Zone, Figure 2b) [*Henkel*, 1991; *Lundin and Doré*, 1997; *Olesen et al.*, 1997; *Fichler et al.*, 1999]. These transfers have also been speculatively linked to fracture zones far offshore that supposedly offset early magnetic anomalies generated during seafloor spreading [*Lister et al.*, 1991; *Tsikalas et al.*, 2001], although the results of new aeromagnetic surveys now question the existence of these oceanic fracture zones that coincide with these “second-order” transfers [*Olesen et al.*, 2005].

[16] Apatite fission track (AFT) data, radiometric dating and onshore analysis all suggest that the basement rocks of Lofoten and Vesterålen experienced similar post-Caledonian histories until the Late Paleozoic [*Hames and Anderson*, 1996; *Klein and Steltenpohl*, 1999]. Subsequently, these two areas appear to have undergone differential vertical movements [*Hendriks and Andriessen*, 2002]. Again segmentation is apparent, with different cooling and denudation histories found throughout the archipelago. AFT analysis in central and north Lofoten and Vesterålen suggest that outer Vesterålen (i.e., Langøya) was exhumed (based on cooling ages) in Permo-Triassic times, whereas analyses in north Lofoten (and possibly also inner Vesterålen) suggest Jurassic-Cretaceous denudation ages [*Hendriks and Andriessen*, 2002; *Hendriks*, 2003], at a time when Langøya was subsiding and covered by sediments [*Davidson et al.*, 2001]. Central Lofoten shows evidence for cooling in Mid-Cretaceous times [*Hendriks and Andriessen*, 2002]. *Hendriks and Andriessen* [2002] proposed that the transfer zones have in some way accommodated these differential vertical movements, although the precise mechanism to account for such movements is not explained.

3. Methods and Data Acquisition

3.1. GIS Database

[17] In any study where both onshore and offshore fault data are examined at a range of scales it will be advantageous to use a Geographic Information System (GIS). GIS is an information system used to input, store, retrieve, manipulate, analyze and visualize geographically referenced

geospatial data [*Longley et al.*, 2001]. In this study we compiled remote sensing, fieldwork and offshore seismic reflection data sets in a single GIS database using the ArcGIS™ suite. All data are geospatially located in a consistent coordinate system (WGS 84 UTM zone 33). This digital workflow forms part of a new in-house mapping methodology, Geospatial Acquisition, Visualization and Analysis (GAVA) [*Clegg et al.*, 2005; *Wilson et al.*, 2005; *McCaffrey et al.*, 2005] which integrates field- and laboratory-based digital mapping methodologies and allows for continual data analysis and evaluation at every stage in the data gathering process.

3.2. Onshore (“Surface”) Data Set

[18] Regional-scale structures have been mapped using remote sensing techniques, particularly lineament analysis, and the digitization of preexisting geological maps. Fault structures at this scale were interpreted from Landsat thematic mapper (TM) data. The application of lineament analysis for the interpretation of geological structures is a well established method that has been widely applied in Norway [e.g., *Gabrielsen and Ramberg*, 1979; *Karpuz et al.*, 1993, 1995; *Gabrielsen et al.*, 2002]. Lineaments were picked from Landsat images along the LVA at a scale of 1:100,000. Attribute data (i.e., trend; length; offset; comments) were also recorded and stored in the GIS database. After interpretation, lineaments were then compared to a digital terrain model (DTM) and refined using GIS analysis. Particular care was taken to avoid the inclusion of basement fabrics in the lineament database. This was confirmed by studying preexisting geological maps during lineament analysis, and was additionally checked during fieldwork.

[19] Outcrop-scale structures were collected using some of the new digital geological techniques outlined by *McCaffrey et al.* [2005]. Digital methods are becoming a common means of field data acquisition [*Maerten et al.*, 2001; *Hodgetts et al.*, 2004; *Jones et al.*, 2004; *Clegg et al.*, 2005]. This is in part because the equipment and software required now meet the needs of the field geologist (e.g., portability, accuracy, versatility, cost, etc. [*Edmondo*, 2002; *Wilson et al.*, 2005]), but also because it is becoming increasingly recognized that having precise geospatially located field data enables efficient 3-D visualization and analysis in ways that are not possible with data collected using traditional paper-based notebook collection methods [*McCaffrey et al.*, 2005]. Gathering outcrop data in digital format (compatible with standard software used in the hydrocarbon industry) is a prerequisite for efficient comparison between onshore and offshore data.

[20] The equipment used for data capture during geological fieldwork in Lofoten comprised the following: (1) a hand-held computer (HP Jornada PDA) equipped with mobile GIS Software; (2) a backpack mounted Differential Global Positioning Satellite receiver (Trimble™ AG122); (3) a laser rangefinder (MDL LaserAce 300); and (4) a digital camera [*Wilson et al.*, 2005]. Field data were recorded in the form of 3-D shape files (containing xyz position), using ArcPad™ (version 6), a mobile GIS software suitable for running on Windows CE devices

[Edmondo, 2002]. Outcrop data (e.g., fault measurements and lithological data) were stored in point shape files, while linear features in map view (e.g., fault trace, traverse line, etc.) were recorded as polylines. These were supplemented by georeferenced outcrop photos and field sketches, both in a digital format. Structures exposed in vertical outcrops (i.e., road cuts) were recorded using a combination of digital photography and 3-D outcrop data capture using a laser ranger (recording xyz point cloud data for outcrop surfaces and fault traces [Xu *et al.*, 2000]).

[21] Field mapping was concentrated on Lofoten's northernmost island, Austvågøya (Figure 2c). This was in part because of the dramatic topography and excellent exposure on Austvågøya.

3.3. Offshore (“Subsurface”) Data Set

[22] During the development of our regional structural database a number of regional offshore fault maps were digitized, including Mokhtari and Pegrum [1992], Blystad *et al.* [1995], Løseth and Tveten [1996], Olesen *et al.* [1997, 2002], and Tsikalas *et al.* [2001]. However, some inconsistencies were found between these data sets (i.e., trends of faults, fault linkage, etc.) and consequently twenty-four 2-D seismic lines (data coverage approximately 100 km × 75 km) were studied for an area west of the Lofoten Ridge (see Figure 6 in section 4.2.1 for location of survey area).

[23] Seismic interpretation was carried out using GeoFrame IESX™ before exporting fault and horizon data to TrapTester™ to construct a 3-D structural model of the area. Five prominent reflectors were mapped, and have been correlated with the intra-Mesozoic, Base Cretaceous, intra-Lower Cretaceous, Aptian and Albian horizons mapped by Tsikalas *et al.* [2001] in the Ribban Basin. Larger faults have been linked with some confidence based on mapped variations in fault throw, and the resulting fault polygon maps have been exported to GIS for comparison with onshore structures, while geometries have been analyzed in TrapTester.

3.4. Building 3-D Models

[24] The 3-D models provide a powerful tool for regional-scale structural investigations. Simple models for the Lofoten Ridge were first constructed in ArcGIS, by overlaying Landsat images for the LVA region onto a DTM (Digital Terrain Model) of the area. These models can be viewed from different vantage points, zoomed to different scales, and simulated “fly through” animations created. This is particularly useful for studying the relationship between structures and topography. Bedrock maps, gravity maps and magnetic maps were also draped onto the DTM for similar studies. These simple models have been described as “2.5-D” representations [Longley *et al.*, 2001; Jones *et al.*, 2004] as they do not provide any direct information about the subsurface geology. For a fully 3-D model (i.e., equivalent to seismic models offshore) structures must be projected into and out of the topographic surface. For this type of analysis, more specific 3-D modeling software is required. Following structural interpretations in GoCAD™, regional 3-D fault models were then reimported into ArcGIS

(ArcScene) for integration with field GIS data and offshore fault and horizon models.

4. Regional Structural Analysis

4.1. Onshore Surface Analysis

4.1.1. Lineament Populations

[25] Along the Lofoten-Vesterålen archipelago, good exposures in crystalline basement and the strong topographic relief permit the ground truthing of lineaments that were mapped using Landsat TM data. The region appears highly faulted and fractured, as indicated by the dense set of 2000 lineaments identified from the remote sensed data [Gabrielsen *et al.*, 2002; this study]. These regional lineament maps show the Lofoten Ridge to have two dominant lineament trends, NNE-SSW (020°–040°) and ENE-WSW (070°–090°) (Figure 3), with subsidiary NW-SE, NE-SW, and E-W trends. Central Lofoten (i.e., Flakstadøya and Moskenesøya) and outer Vesterålen both show dominant N-S and NNE-SSW oriented lineament suites, while an ENE-WSW trending lineament suite can be seen in north Lofoten (Vestvågøya and Austvågøya) running east toward Ofotfjorden (Figures 3a and 3b). Other systems include a NW-SE trending suite on Vesterålen (Figures 3a and 3b).

4.1.2. Lineament Domains

[26] Using ArcGIS, lineament density maps were made by counting the total number and total length of lineaments within a moving 1 km² search window. These maps highlight the dominant lineament in different parts of the LVA. Directional analysis was also carried out using rose diagram plotting tools in ArcView. Having gridded the area into 10 km × 10 km cells, rose diagrams were plotted for each cell (Figure 3c). These spatial analyses reveal that the LVA can be subdivided into a series of distinct lineament domains: (1) central Lofoten (CLD), (2) north Lofoten (NLD), (3) Lødigen (LøD), (4) Hinnøya (HinD), and (5) Langøya (LangD); Figure 3d). In all 5 domains, a dominant lineament trend is NNE-SSW to NE-SW, with some domains also showing a second dominant trend: ENE-WSW in north Lofoten, and NW-SE on Hinnøya. These domains are coincident with changes in ridge trend, and with previously documented variations in regional gravity and magnetics (Figures 4b and 4c), but also denudation ages and offshore fault patterns [Tsikalas *et al.*, 2001; Hendriks and Andriessen, 2002; Olesen *et al.*, 2002]. Gravity highs appear to be associated with domains showing a single preferred lineament trend (i.e., central Lofoten and Langøya domains [see Olesen *et al.*, 2002, Figure 10]).

4.1.3. Detailed Lineament Studies on Austvågøya

[27] Figure 4 shows a more detailed view of the multimodal lineament trends seen on Austvågøya (north Lofoten). In this area 4 main lineament systems have been identified: approximately N-S (system 0); NNE-SSW to NE-SW (system 1); ENE-WSW to E-W (system 2); and ESE-WNW to SE-NW (system 3).

[28] System 0 lineaments (S0, Figure 4) are represented by deep, wide valleys and fjords, showing characteristics of classic glacial U-shaped valleys. Compared to other systems, this system has a relatively wide spacing (roughly

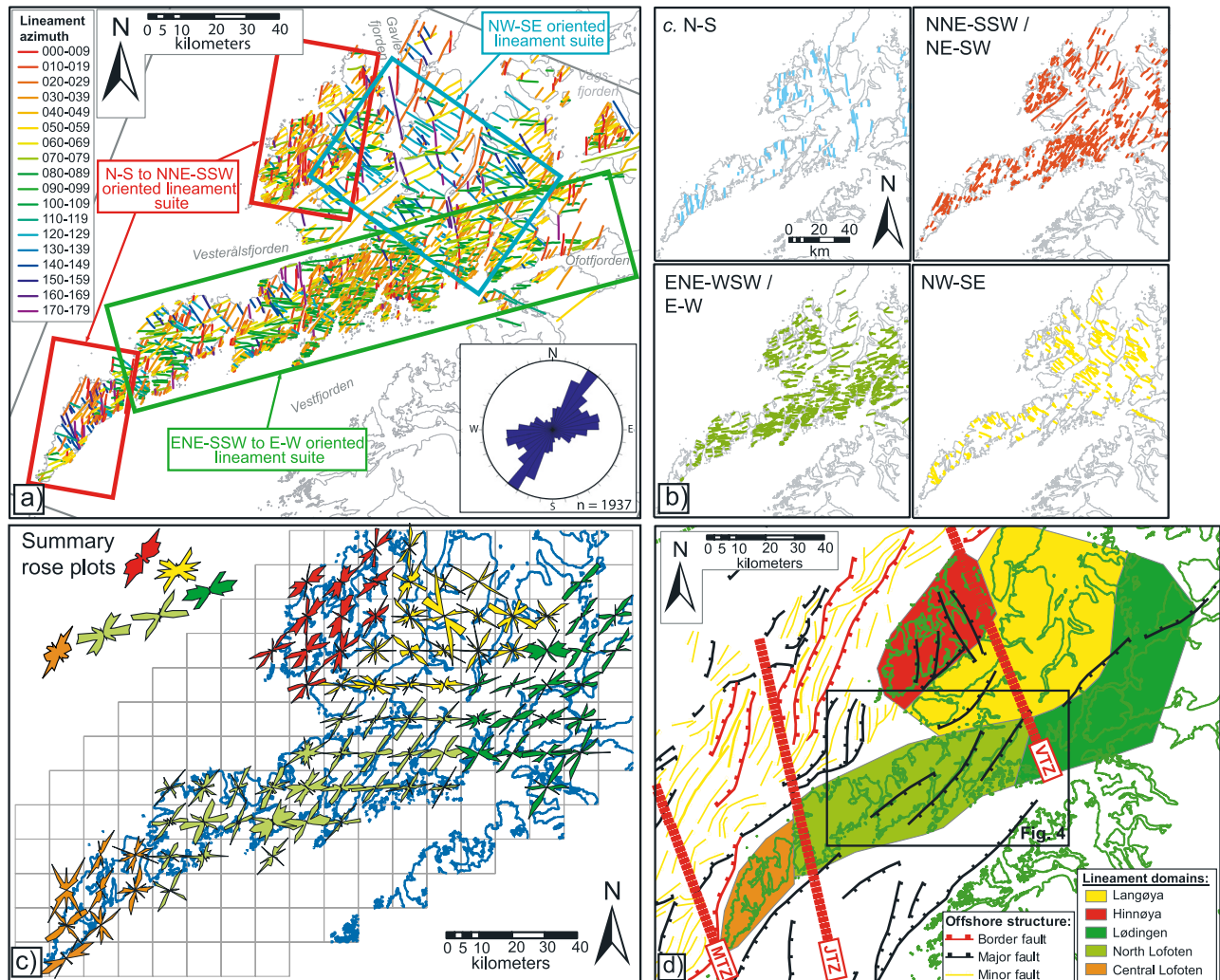


Figure 3. Regional lineament analysis of satellite data for the LVA. (a) Landsat TM image with structural lineaments mapped at 1:100,000 scale, plus a rose diagram highlighting dominant lineament trends. (b) Lineament maps showing distribution the four main lineament systems identified in Lofoten (N-S; NNE-SSW/NE-SW; ENE-WSW/E-W; NW-SE). (c) Rose diagram map for lineaments. Map gridded in to 10 × 10 km squares, with corresponding rose diagrams plotted for each square. Plots are colored according to similarities in trend. Plots in top left show summary plots for changes in lineament trend along the ridge. (d) Lineament domains identified from spatial analysis using GIS (i.e., lineament density maps for each lineament trend and rose diagram maps shown in Figure 3c).

every 3–5 km), and as a result there are fewer S0 lineaments to be observed. However, they do form the largest valleys, and also appear to separate the largest islands (i.e., Flakstadøya, Vestvågøya, Austvågøya). Wide N-S valleys (S0) often appear bend, or be offset, in a counterclockwise/left lateral sense. This later deformation may suggest that S0 lineaments are relatively old structures.

[29] System 1 lineaments (S1, Figure 4) are the most common lineament trend along the ridge and are characterized by narrow, deeply incised valleys and fjords, such as Raftsundet (Figure 4c). System 2 lineaments (S2, Figure 4) have a similar geomorphologic style to S1, i.e., represented by arrow, steep sided valleys such as the famous Trollfjord (Figure 4d). A distinct change in trend of S2 lineaments

(from ENE-WSW to E-W) can be seen across Austvågøya (Figure 4). This change appears to roughly match a change in the trend of the overall ridge.

[30] A strong correlation between the change in trend of S2 and the frequency and orientation of S1 lineaments is also apparent. The density of S1 appears higher where S2 lineaments trend E-W, and the mean orientation of S1 lineaments in this same zone also appear to be $\sim 10^\circ$ clockwise of S1 trends farther to the southwest (Figure 4). Crosscutting relationships observed between S1 and S2 lineaments appear to be quite complex, with good examples of both S2 cutting S1 and vice versa. This mutual crosscutting relationship is likely to suggest that

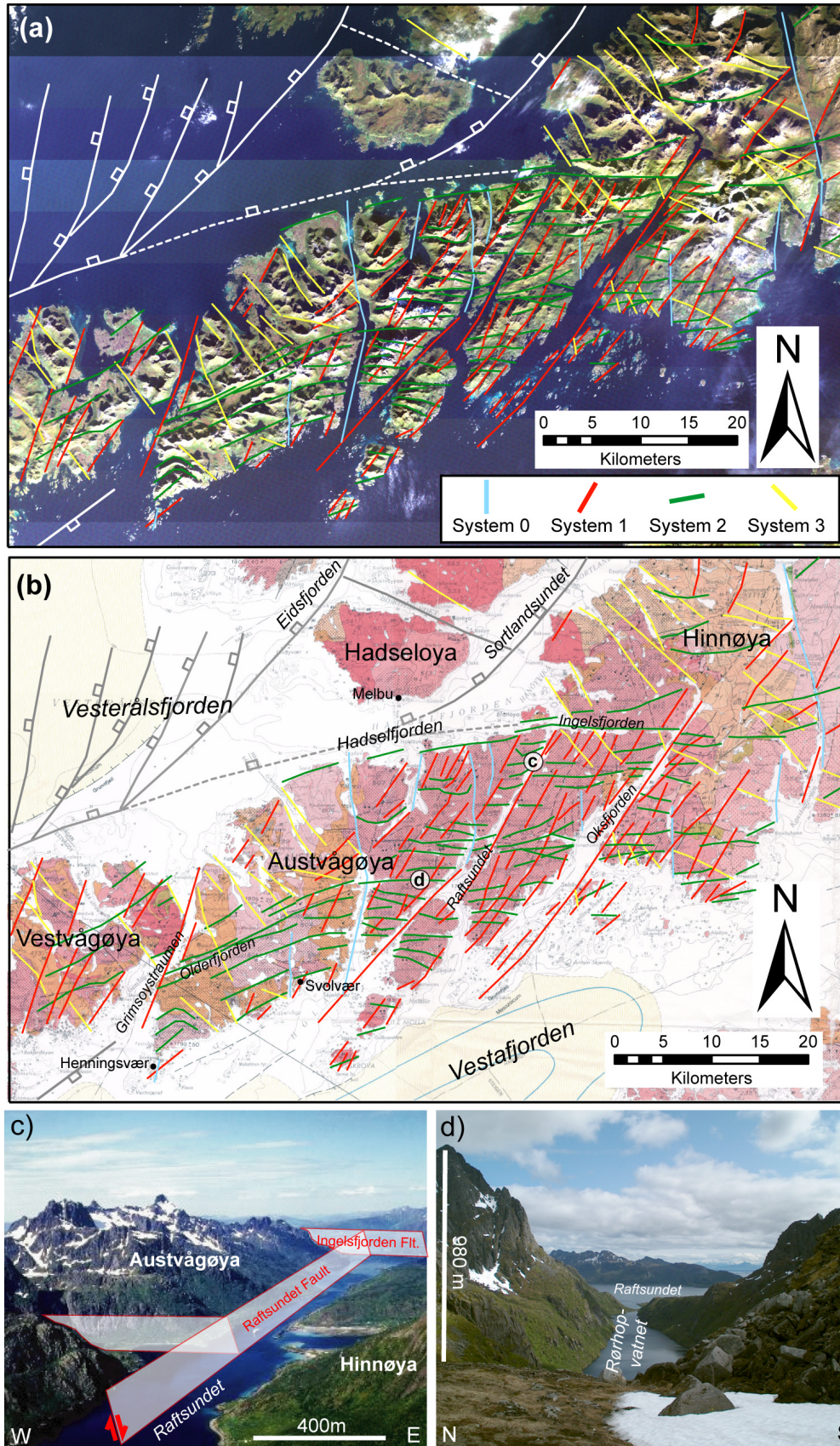


Figure 4

these systems formed, or were active during the same tectonic event.

[31] System 3 (S3, Figure 4) is most pronounced on Vesterålen; however, a number can also be seen cutting the Lofoten Ridge. These lineaments are represented by both narrow and wide valleys. Crosscutting relationships suggest that S3 lineaments are the youngest system as they appear to truncate most other trends, although caution must be taken when interpreting age relationships from lineaments as it is often unclear if truncations represent lineament terminations or true crosscutting older by younger.

4.1.4. Regional Onshore Structural Model

[32] The 3-D fault models have been created for these lineament maps in an attempt to construct onshore models equivalent to those produced from offshore seismic studies. This was done using structural modeling tools in GoCAD™ by overlaying Landsat lineament interpretations (in vector form) over a 50 m DTM; the lineaments then take on a 2.5-D configuration (a curved line in 3-D space). If there is sufficient interaction between topography and the lineament trace (the considerable topographic relief of Lofoten is perfect for this), then best fit surfaces can be constructed along each lineament, thus producing a representative fault plane (see Figure 5). Not only does this method provide a model to help visualize the 3-D structure of the region, but also allows the strike and dip of these regional fault surfaces to be calculated. These faults can then be compared to the equivalent geometries interpreted from offshore seismic data and to field data (Figure 5).

[33] The 3-D fault models were created using this method over a 25 km × 50 km area of north Lofoten (Figures 4 and 5). Like the rest of the NLD, lineament orientations in this area have two distinct preferred orientations, ~035°–215° (S1) and ~080°–260° (S2). The resulting 3-D model for these structures displays a rhombic fault block pattern (Figure 5), while the poles to planes of these regional structures appear to cluster in a bimodal distribution (Figure 5f). Because of the lineament picking method favoring straighter lines (i.e., the picker is nearly always biased toward drawing straighter lines, particularly across areas of uncertainty, such as hillslopes in shadow or less distinct lineament trace), the faults may appear steeper than they really are (because a straighter line equates to a steeper structure), which may account for the apparent clustering around the vertical dip.

4.2. Offshore Subsurface Analysis

4.2.1. Offshore Central Lofoten and the Havbåen Subbasin

[34] Offshore central Lofoten is characterized by a single major NNE-SSW to NE-SW trending border fault (parallel to the ridge trend) bounding a large depocenter (the Havbåen subbasin; Figures 6a and 6b). Synrift thick-

ening of Upper Jurassic and Lower Cretaceous sequences is apparent along the West Lofoten Border Fault (WLBF) in this area, while most Middle Cretaceous sediment infilling the Havbåen subbasin appears to be associated with thermal subsidence, thickening toward the center of the basin. Intra-Lower Cretaceous and Middle Cretaceous hanging wall sequences dip away from the WLBF before shallowing to horizontal through a hanging wall syncline (Figure 6a). Overlying strata can be seen to onlap these tilted horizons (see profile F, Figure 6b). This geometry resembles a similar compaction-related geometry discussed by Thomson and Underhill [1993] for faulting in the Moray Firth. These structures are interpreted to form in response to differential compaction as a consequence of varying hanging wall and footwall lithologies together with a buttressing effect created by the underlying rigid footwall. Further synrift thickening of Upper Cretaceous sediments appear restricted to the deepest part of the basin (see profile F, Figure 6a).

4.2.2. Offshore North Lofoten

[35] Offshore north Lofoten shows a number of contrasting structures and styles compared those observed farther south. First, the throw on the WLBF appears to decrease markedly, which has resulted in a much shallower basin in this area. Furthermore, the WLBF also shows a distinct change in trend in this area, bending round into a NE-SW to ENE-WSW orientation (Figures 6b and 6d). A number of NNE-SSW trending, west dipping normal faults (green faults in Figure 6) appear to bend round and join the WLBF (Figures 6b and 6d). These have been interpreted as a system of en echelon faults splaying off the border fault as it bends round in to an ENE-WSW trend. Alternatively they may represent a system of breached relays. Either way, these imply a component of sinistral oblique extension along the WLBF in this area. These splay faults cut Late Jurassic and Base Cretaceous strata. Also characteristic of this area are a number of major NNE-SSW trending, east dipping faults located farther offshore (yellow faults in Figure 6). These show extensive synrift thickening of hanging wall sequences of Late Jurassic to Mid-Cretaceous (Aptian) age (Figure 6a). These faults lie along strike from the prominent WLBF bounding the central Lofoten segment and likely take up much of the extension not seen along the border fault as it is traced northward.

[36] Throws on the WLBF and associated faults are reduced compared to those seen farther south, and more faults can also be seen cutting lower Cretaceous strata. This may suggest that deformation is less focused along the bounding fault in north Lofoten and that strain is more distributed across the basin. Further to this observation is the fact that there is no significant depocenter in this area compared to central Lofoten and there is also significantly less evidence for thermal subsidence and infilling (Figures 6a and 6b). In the northern part of this area,

Figure 4. (a) Detailed lineament studies of north Lofoten. Lineaments are colored according to fault/lineament system (S0–S3). Offshore trends are adapted from *Løseth and Tveten* [1996] and results of this study. Dashed lines show inferred link up of faults. (b) Lineament trends plotted on geological map of Lofoten [*Tveten*, 1978]. (c) Oblique aerial photograph of Raftsundet (S1), looking north. (d) Photograph of E-W trending narrow, steep sided valley (S2), truncated by Raftsundet, looking east.

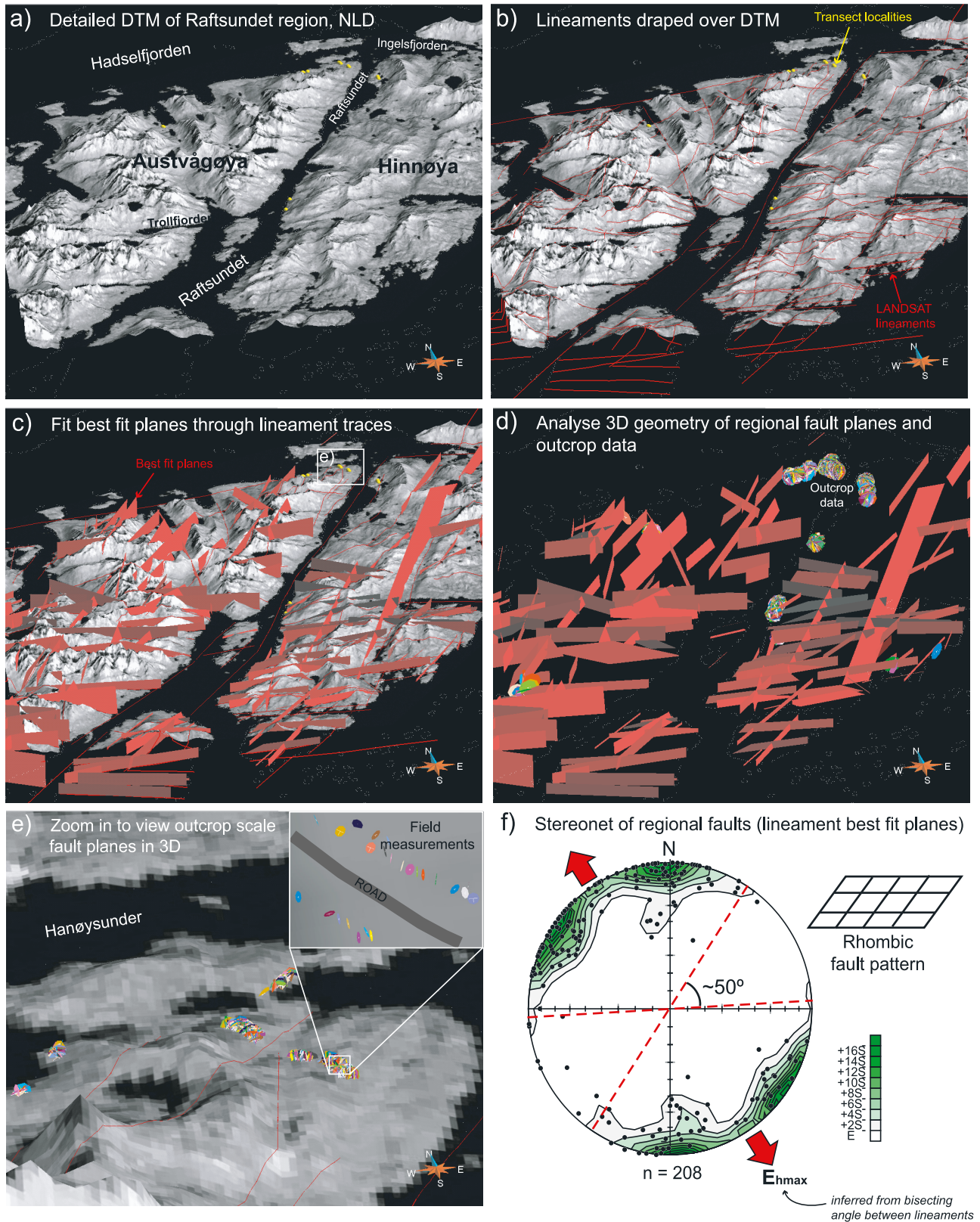


Figure 5

sedimentary sequences appear to have been uplifted and eroded. This is likely to have occurred at the same time as the sediments that covered Vesterålen were eroded away [Dalland, 1981; Løseth and Tveten, 1996].

[37] A NNW-SSE trending transfer zone (Jannegga transfer zone [Tsikalas *et al.*, 2001]) has previously been mapped through the area between these two domains. However, it should be noted that no distinct structures marking the position of this transfer zone can be seen in seismic data (see Figure 6a), and thus this zone simply marks the transition between domains of differing fault polarity and basin location.

5. Field Data Analysis

5.1. Outcrop Exposures Around Raftsundet

[38] Field reconnaissance mapping in north Lofoten (Austvågøya and Vestvågøya) has confirmed that most lineaments correspond to major fault structures (Figures 4c and 4d). In some cases the structures themselves cannot be directly identified as they lie at the bottom of fjords or vegetated valleys (e.g., Raftsundet; see Figures 4c and 7a). However, the intensity of fracturing in adjacent areas of exposed rock is consistent with their location close to major fault structures. Almost all exposures in the mapping area were in charnockites (orthopyroxene granite) and mangerites (orthopyroxene monzonite) of the Raftsund Pluton (colored pink in Figure 4b). These rocks exhibit a weak E-W trending fabric; however, in many places, basement fabrics were indiscernible. The freshest exposures of fault surfaces were found on road cut sections and shorelines; however, because of the dramatic topography of the area, many faults and fault zones can also be easily traced up mountainsides (Figure 7b). Fault exposures varied from large solitary faults in a relatively undeformed country rock (Figure 7c) to fault zones of highly fractured rock (Figures 7d and 7h). Fault rocks observed were generally semibrittle (slickenlines) to brittle (cataclasite) (Figures 7d and 7e), and little evidence for fluid interaction during deformation was observed (the only example of mineralization was found at a locality in the hanging wall of the Ingelsfjorden fault, in the form of epidotic slickenfibers).

5.2. Fault Populations

[39] During fieldwork, 666 mesoscale (centimeter-decimeter scale exposures) faults and fractures and associated slip striae have been measured at over 20 localities across NE Austvågøya. More than 60% of the faults measured exhibit good kinematic indicators, in the form of slickenlines and striated coatings (Figure 7e). Kinematic

indicators such as Riedel shears were used to infer shear direction and shear sense on each fault plane [Petit, 1987].

5.2.1. Steep Brittle Faults

[40] When plotted stereographically, three main brittle fault clusters are apparent (Figure 8a, left), with strike orientations that closely match the data derived from lineament analysis (Figure 5f). These clusters reflect 2 distinct fault geometries: (1) NNE-SSW to NE-SW trending faults, dipping NW and SE (system 1/S1; Figure 8b) and (2) ENE-WSW to E-W trending faults dipping mainly to the north (system 2/S2; Figures 7b and 8c). These fault geometries are matched by similar fracture/joint trends (i.e., surfaces with no clear evidence for shear; Figure 8a, right). Only ENE-WSW and E-W trending surfaces showed plumose markings characteristic of joints (Figure 7g), and these were found in the vicinity of an E-W trending lamprophyre dike at locality LO3 (the margins of which have been reactivated by sinistral strike-slip movements; Figures 9a and 10). A second lamprophyre dike trending NNE-SSW was also observed at Locality LO2 (Figure 9b), in this case the dike was highly deformed and reactivated by both dip-slip and dextral oblique-slip faults. Plots of slip striae (Figure 8a, middle) show that all fault orientations are dominated by dip-slip (i.e., slickenline pitch $>60^\circ$) or oblique-slip (pitch 30° – 60°) normal fault movements. However, a small number of strike-slip (pitch $<30^\circ$) movements were also observed, and some faults also exhibit multiple slip striae. Strike-slip striae on system 1 (NNE-SSW oriented) faults indicate a dextral shear sense; while on system 2 (ENE-WSW oriented) faults show sinistral shear, and may represent a conjugate pair (Figure 8d).

[41] A spatial analysis of fault geometry and slickenline data was carried out in ArcView using an interactive GIS stereoplot program provided by Knox-Robinson and Gardoll [1998]. Figure 10 shows a summary map, and associated stereonet, for fault populations for localities in the area of Raftsundet. No distinct patterns of spatial distribution are apparent across the mapping area; however, it may be noted that fault geometries at outcrop generally reflect local lineament trends. At a number of localities, there also appears to be a strong correlation between the dominant slickenlines orientation and the mean fault intersection (Figure 10).

5.2.2. Low-Angle Normal Faults

[42] A number of low-angle ($<45^\circ$ dip) normal faults can be found in the vicinity of Raftsundet (e.g., localities LO9, 10 and 11; Figure 10). These generally dip to the west and northwest and have a listric geometry. These faults are characterized by a deformation zone (50–200 cm thick) of ductile (mylonitic) to semibrittle fault rocks (Figure 7f). Similar structures have been described by Heier [1960] and Løseth and Tveten [1996] on Hinnøya and Langøya to the

Figure 5. (a) A 2.5-D model of the Raftsundet region, Austvågøya, north Lofoten, comprising a Landsat image draped over DTM. (b) Lineaments (vector data) imported from ArcGIS and draped over DTM. (c) Best fit planes fitted through 3-D lineament traces to produce a 3-D fault model. (d) Regional and outcrop-scale fault planes analyzed in same 3-D model. (e) Fault planes at outcrop. Fault geometries are recorded as point data in the field using digital mapping methods. (f) Equal-area lower hemisphere stereoplot of regional fault planes derived from best fit planes through 3-D lineament traces. All models are constructed using GoCAD.

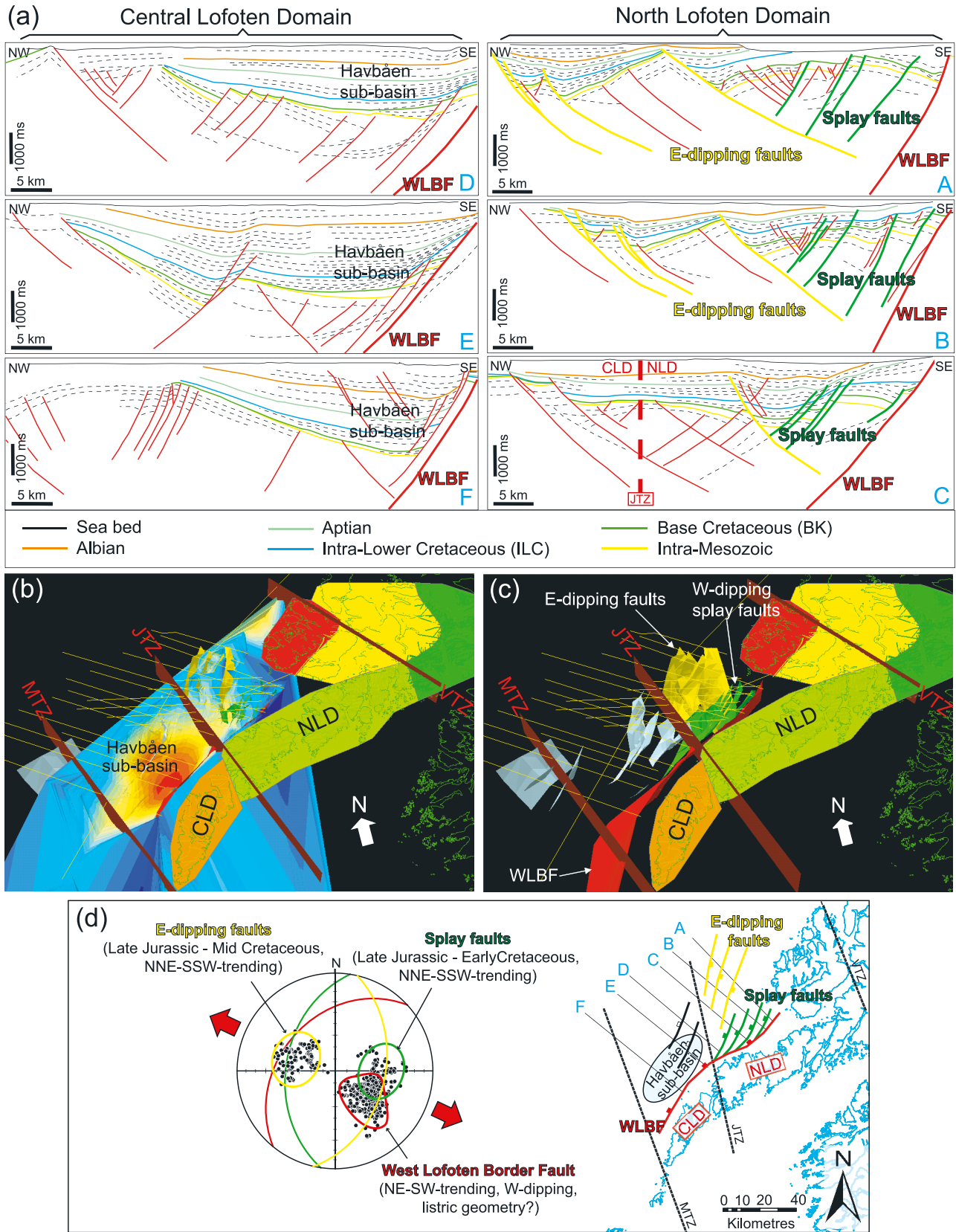


Figure 6

north. These faults are important as they appear to be locally reactivated by later brittle faults described above (Figure 7).

5.3. Age Relationships

[43] Both crosscutting fault relationships and overprinting slickenline have been analyzed in an attempt to determine a temporal succession of fault movements. A younging table (Table 1) was constructed using methodology of *Potts and Reddy*, [1999] in order to determine the relative age relationships of each fault set based on the field observations (e.g., crosscutting relationships and overprinting fault striae; Figure 7f). For the interpretation of age relationships faults have been categorized into six distinct systems based on orientation and slip: NNE-SSW (normal); NNE-SSW (strike slip); ENE-WSW (dip slip); ENE-WSW (strike slip); NE-SW (oblique slip); low-angle normal faults.

[44] Only a few conclusive and consistent crosscutting relationships between faults can be identified. Low-angle normal faults are clearly the oldest faults observed, with NNE trending (S1) faults appearing to be next, followed by ENE-WSW (S2) and NE-SW. However, the relationship between S1 and S2 faults appears far more complex with examples of S1 faults crosscutting S2 faults, and vice versa, being seen within any one exposure. This mutual crosscutting relationship therefore likely suggests that these fault systems developed at a similar time or at least were active during the same tectonic event. It should be noted that strike-slip striae appear to postdate dip-slip striae on most NNE-SSW trending (S1) fault surfaces; however, the relationship between dip-slip and strike-slip movements on S2 faults is more unclear. In many cases, multiple slickenlines on a single fault surface can be attributed to fault interaction rather than reactivation (see Figures 9c and 9d and section 5.5).

5.4. Kinematic Analysis

[45] Kinematic analysis was carried out using so-called “paleostress analysis” techniques. The analysis of fault slip data yields information concerning the orientation of the strain tensor, and thus the calculated axes are referred to using infinitesimal/finite strain nomenclature rather than principle stresses. The aims of our study here were (1) to determine if all fault movements are compatible with a single strain field and (2) to derive a “paleostress” tensor from the outcrop data that can be compared to kinematics inferred from regional fault patterns developed onshore and offshore. Kinematic inversion techniques have been extensively

used by various workers for nearly 40 years (see *Angelier* [1994] and *Ramsay and Lisle* [2000] for an exhaustive review). The assumptions and methods of paleostress have been discussed in detail in many other papers [*Éthecopar et al.*, 1981; *Angelier*, 1984, 1994; *Michael*, 1984; *Reches*, 1987; *Delvaux and Sperner*, 2003] and are not discussed here. It should be noted, however, that this approach is reasonable only in regions where there is little misorientation between finite and infinitesimal strain axis (i.e., in areas where finite noncoaxial strain is low).

5.4.1. Inversion Procedures

[46] In total, 414 faults with good kinematic indicators were recorded (Figure 8a), which can be used for kinematic inversion. My Fault™ stereonet software, produced by Pangaea Scientific Ltd., was used for kinematic analysis.

[47] Two separate procedures for sorting the fault data into populations for inversion analysis have been applied during the present study. The first (procedure 1) simply uses the entire unsorted data set (i.e., all 414 fault and fault striae) while the second (procedure 2) required manual sorting and separate analysis of the data into fault systems.

[48] In procedure 1, after input of the raw data, data files were corrected to ensure that all striae lie perfectly on their respective fault planes (i.e., no angular mismatch). To do this, fault striae were rotated along the common plane containing the striae and the pole of the fault plane. Following this, the bulk fault population data set was inverted. Those faults with high misfit angles (>40°) relative to the inversion result were then rejected and the inversion rerun. This procedure was repeated until a single group of faults with a homogeneous solution could be found. The rejected data were then rerun through the program in an attempt to derive multiple paleostress vectors. A similar iterative approach has been applied by *Titus et al.* [2002]. This procedure was then repeated for various inversion methods [i.e., *Angelier*, 1984; *Michael*, 1984; *Reches*, 1987] to test the consistency of the results.

[49] In procedure 2, a potential risk when analyzing a bulk fault population data set with uncertain age relationships is that the kinematic data being analyzed represent more than one phase of movement. This can result in the derived vectors reflecting a combination of the two or more phases and may not be geologically meaningful [*Delvaux and Sperner*, 2003]. Fault data were separated according to fault geometry (i.e., fault systems 1 and 2; Figures 8b and 8c), and any examples of structures associated with fault interaction were disregarded as this violates the basic assumptions of inversion methods [*Nieto-Samaniego and*

Figure 6. (a) A series of interpreted seismic profiles, trending NW-SE, across the Ribban Basin. Profiles highlight changes in basin geometry and fault style between central Lofoten and north Lofoten. (b)–(c) Onshore-offshore 3-D models in ArcGIS (ArcScene). Figure 6b is a base Cretaceous horizon map showing a large depocenter (the Havbåen subbasin) offshore central Lofoten, and no basin apparent in north Lofoten. Figure 6c shows a fault model showing distinct change in geometry from south to north Lofoten (red, WLBF; green, splaying faults; yellow, low-angle east dipping faults; blue, other minor faults). Also shown are onshore lineament domains (colored polygons) and NNW-SSE trending transfer zones (red planes). Figure 6d is a stereonet (poles to planes) of faults picked in seismic (dips calculated using an interval velocity of 3000 m/s; readings taken every 1 km), plus base map showing location of seismic lines, fault trends, and “transfer zones.”

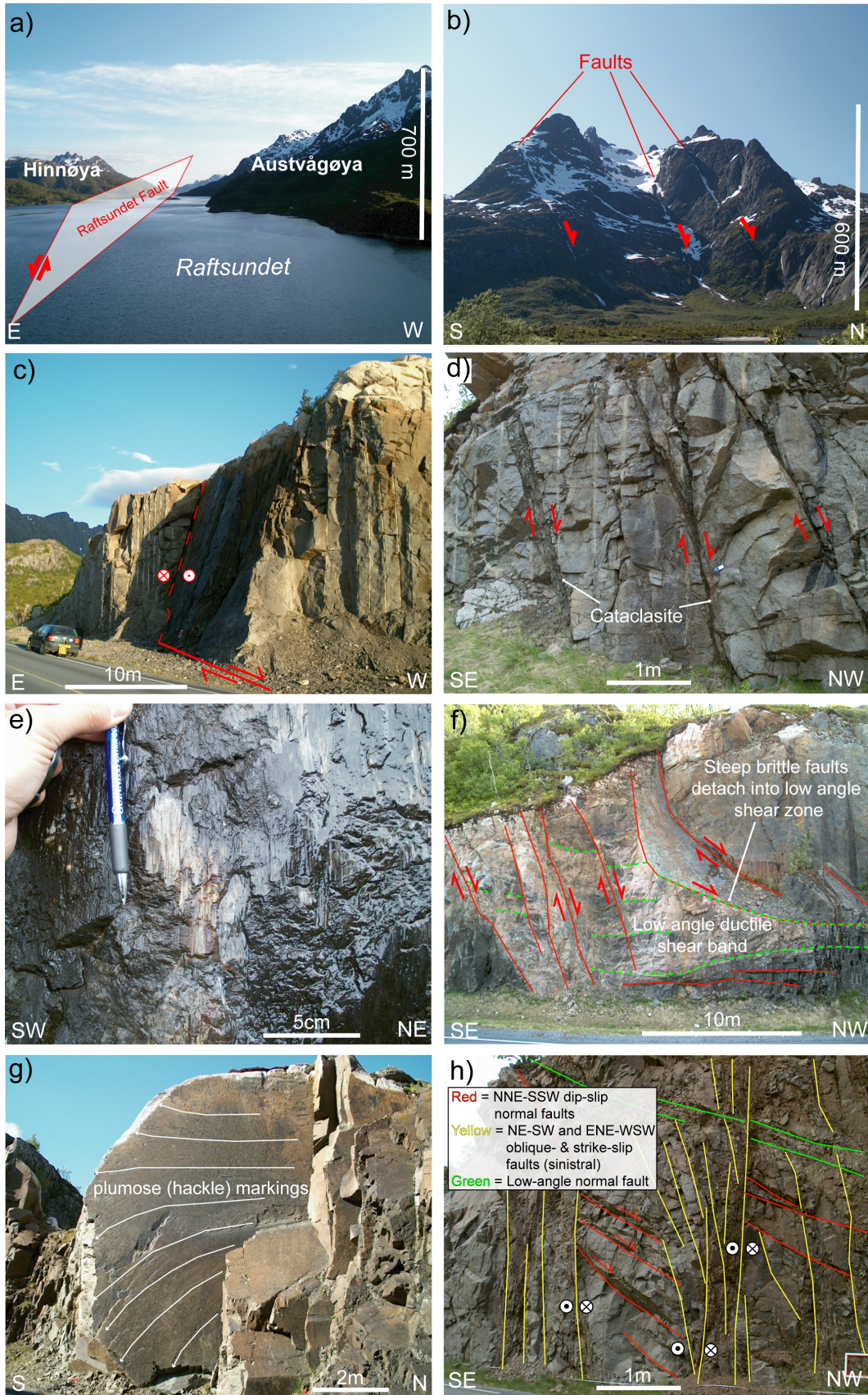


Figure 7

Alaniz-Alvarez, 1997]. As the data have already been sorted prior to analysis, the “iterative” sorting approach, used during procedure 1, was only required for the strike-slip fault set.

5.4.2. Inversion Results

[50] Bulk inversion of all fault data (procedure 1) using the inversion method of *Michael* [1984] produced a sub-horizontal maximum infinitesimal extension strain axis ($x_i \equiv \sigma_3$) of 316/03, and subvertical minimum infinitesimal extension (or shortening) strain axis ($z_i \equiv \sigma_1$) of 170/86, and thus suggests that maximum horizontal extension (E_{hmax}) was oriented NW-SE (Figure 11a). Similarly oriented axes were calculated using all other inversion methods [e.g., *Angelier*, 1984; *Reches*, 1987].

[51] Following procedure 2, three separate sets of paleostress axes can be derived, one for each fault system analyzed (i.e., system 1 dip-slip, system 2 dip-slip, and all strike-slip faults; Figures 8b–8d). Analysis of each fault system yield similarly oriented axes (of course, for strike-slip faults the y_i and z_i axes are switched; i.e., Z is horizontal); although there is a 12° variation in the azimuth of the extensional axes (x_i) (Figure 11b). These results are all consistent with a NW-SE maximum horizontal extension (E_{hmax}), which is roughly 60° to the trend of the north Lofoten Ridge (i.e., in mapping area ridge trends approximately E-W).

5.5. Fault Interaction: Implications for Stress Inversion

[52] In recent years, a number of studies have examined the limitations of inversion methods [*Pollard et al.*, 1993; *Cashman and Ellis*, 1994; *Nieto-Samaniego and Alaniz-Alvarez*, 1997; *Maerten*, 2000]. Slickenlines are kinematic indicators (slip vectors), and when these are used to interpret the regional stress field a number of assumptions have to be made. One of the most important assumptions is that the slickenlines are produced by the general stress tensor, implying that faults do not interact and that the stress field is not significantly perturbed after fault slip. *Pollard et al.* [1993] discuss how interaction between preexisting planes can lead to stress field perturbations of up to 40° in orientation when the density of fault planes is high. Interacting fault movements on preexisting planes can lead to multiple slickenline sets forming under a single regional stress field [e.g., *Cashman and Ellis*, 1994].

[53] In some areas of north Lofoten there is strong evidence to suggest that fault interaction has played a

significant role in the development of faults. As there are multiple fault orientations, and the spacing between faults is small (generally <2 m) some interaction between structures is likely. The mean slickenline orientations at many outcrops appear to coincide with the mean intersection between faults (e.g., Figure 10), which is consistent with the interacting block model of *Nieto-Samaniego and Alaniz-Alvarez* [1997]. Several examples of exactly this type of fault interaction have been recognized at outcrop (e.g., Figure 9c). Another example of interaction between faults is shown in Figure 9d. Here we see a continuous set of slickenlines that can be traced round a 90° bend, from an approximately N-S trending fault plane to one trending approximately E-W. The intersection between these planes appears well rounded, thus suggesting shear along these planes was directly linked. Fault movements suggest a counterclockwise rotation about a subvertical axis (note fault intersection plunges steeply toward the NE; Figure 9d), and are consistent with NW-SE extension with potentially a component wrench simple shear.

[54] *Nieto-Samaniego and Alaniz-Alvarez* [1997] have suggested that fault systems controlled by fault block interaction may not be suitable for paleostress analysis as a number of basic assumptions of these methods are violated. However, given the large number of data collected in the present study and the seeming consistency of the paleostress analysis results, we feel that in this case, a valid result has been obtained. One reason for this is that using a GIS for data management allowed efficient, quantitative filtering of all data points that do not meet certain geospatial or geological criteria. For example, all faults showing outcrop evidence for “fault interaction” were removed from the analysis.

[55] Furthermore, detailed analysis of fault movements associated with these examples of fault interaction indicate that kinematics appear consistent with stress axis interpreted using paleostress analysis described above (Figure 9).

6. Discussion

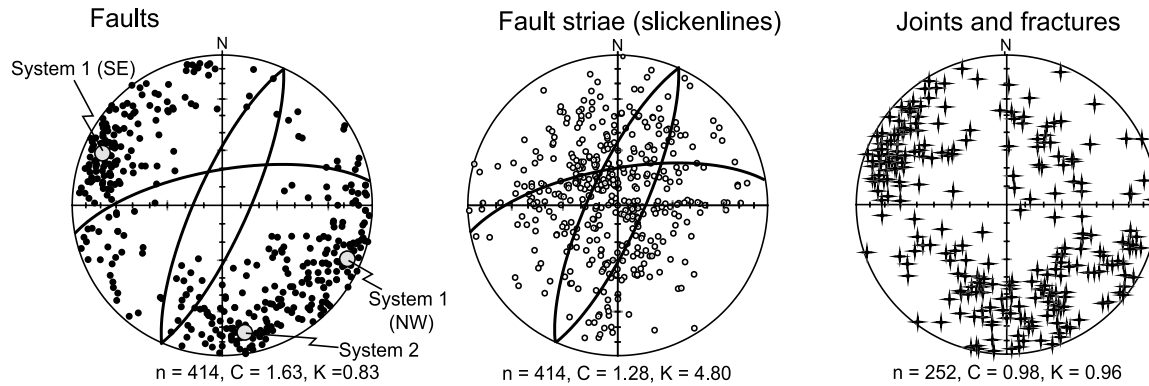
6.1. Structural Variations Along the Lofoten Ridges

6.1.1. Variations Between Onshore and Offshore Structures

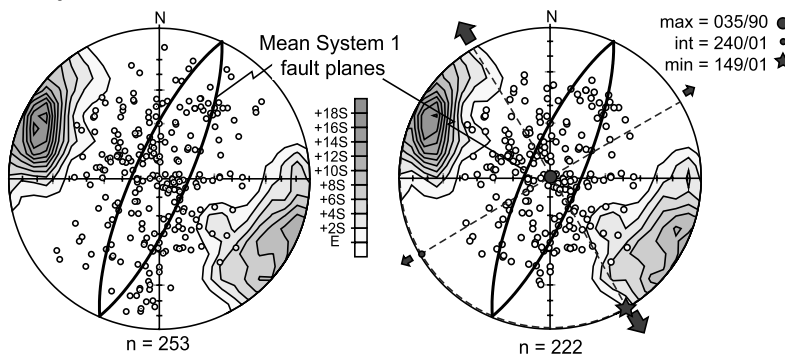
[56] Detailed onshore lineament studies have revealed that the LVA can be divided into a series of distinct lineament domains (Figure 3). These variations are coinci-

Figure 7. Photographs showing regional to outcrop-scale structures seen in Lofoten. (a) Raftsundet, believed to mark the trace of a major SE dipping fault (based on topographic contrasts either side of fjord, and also dominant dip direction of outcrop-scale faults; see Figure 8). (b) Lineaments picked from Landsat images are easily identifiable in the field, faults shown are S2 lineaments. (c) Good example of fault exposure seen in field, example shown is a N-S trending dextral oblique slip/strike-slip fault. (d) NW dipping system 1 faults containing cataclasite fracture bands, associated slip striae show dip-slip and dextral oblique-slip movements. (e) Dip-slip extensional slickenlines (striae) on system 1 faults. (f) Low-angle ductile shear zone showing mylonite shear bands dipping to NW, similar to Devonian detachments described by *Heier* [1960] and *Løseth and Tveten* [1996] farther north in Vesterålen. Brittle faults appear to locally reactivate/detach into these shear bands. (g) E-W trending joint with ornamentations that closely resemble plumose markings [*Hodgson*, 1961]. (h) Complex fault exposures near Raftsundet, from which crosscutting relationships may be observed (in this case, S2 cutting S1).

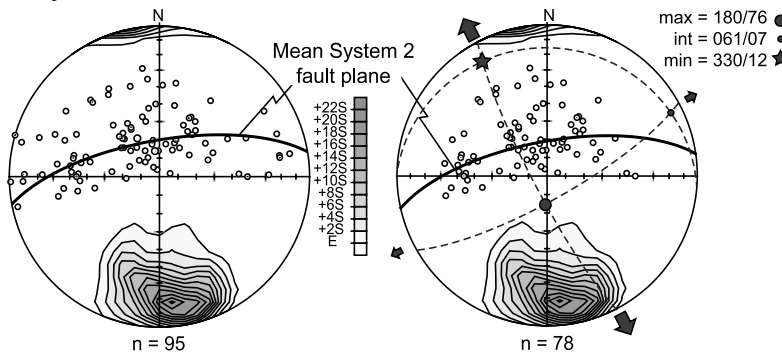
a) Structural data collected during fieldwork



b) System 1 faults



c) System 2 faults



d) Strike-slip faults

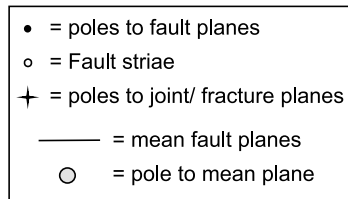
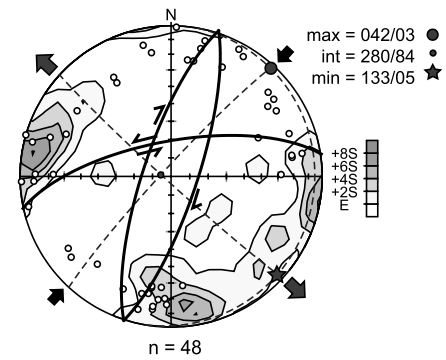


Figure 8. Equal-area lower hemisphere stereonets of structural data from Austvågøya, north Lofoten. (a) (left) poles to planes for all faults recorded in the field, (middle) slickenline lineations on these faults, and (right) poles to planes for joints and fractures. (b) Stereonets for system 1 faults (NNE-SSW/NE-SW trending) showing (left) contours of poles to planes, plus all associated slickenlines (points), and (right) dip-slip slickenlines, plus paleostress axes (calculated using procedure 2). (c) Stereonets for system 2 faults (ENE-WSW trending) showing (left) contours of poles to planes, plus all associated slickenlines (points) and (right) dip-slip and oblique-slip slickenlines, plus paleostress axes (calculated using procedure 2). (d) Combined strike-slip slickenlines for systems 1 and 2, plus paleostress axes (calculated using procedure 2). Data included on each plot are number of data (n) and eigenvector ratios reflecting “strength” (C) and “shape” (K) of preferred orientation.

dent with changes in ridge trend and physiography (i.e., landscape, topography, etc). In central Lofoten (CLD) the trend of the ridge is NNE-SSW, whereas in north Lofoten (NLD) the trend of the ridge is closer to ENE-WSW and is

also much broader. In this northern segment the lineament patterns appear more complex than those to the south. These changes onshore are consistent with important structural changes offshore. The WLBf bounding the central Lofoten

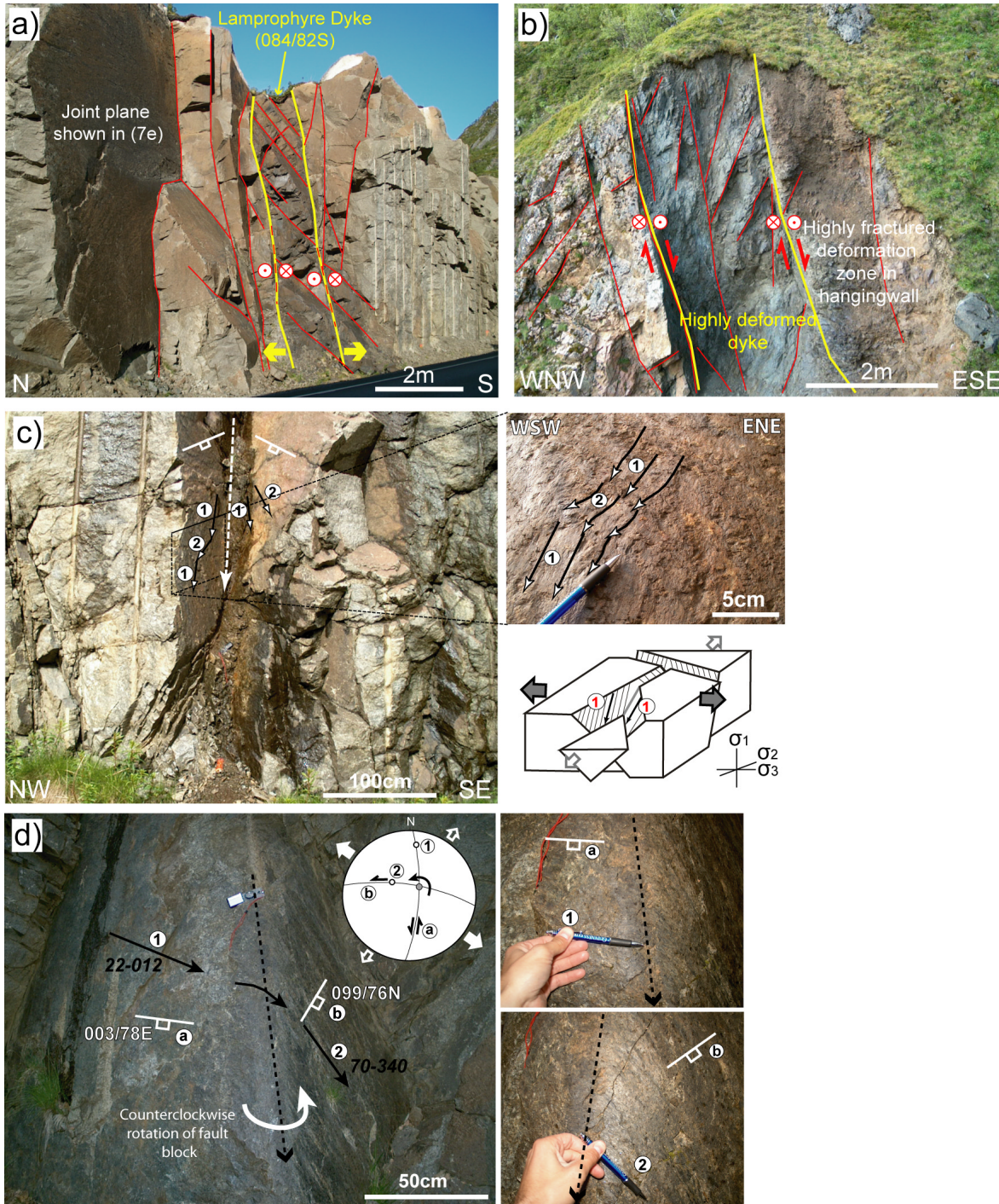


Figure 9. (a) Lamprophyre dike at locality LO3 (see Figure 10 for locality map) trending parallel to system 2 faults and joints shown in Figure 7g. Dike margins reactivated by sinistral strike-slip faults movements. (b) Second dike exposure (locality LO2, Figure 10) trending NNE-SSW, again reactivated by later fault movements. (c) Outcrop photo showing a good example of fault interaction between intersecting faults (locality L06; Figure 10). Note stepwise trend of slickenlines, with a set running parallel to fault intersection line, which is comparable to the interacting block model of *Nieto-Samaniego and Alaniz-Alvarez* [1997]. (d) Second example of complex fault interaction (also locality L06), showing a continuous set of slickenlines that can be traced round a 90° bend, from an approximately N-S trending fault to an approximately E-W fault. Fault movements suggest a counterclockwise rotation about a subvertical axis and are consistent with NW-SE extension associated with a component wrench simple shear.

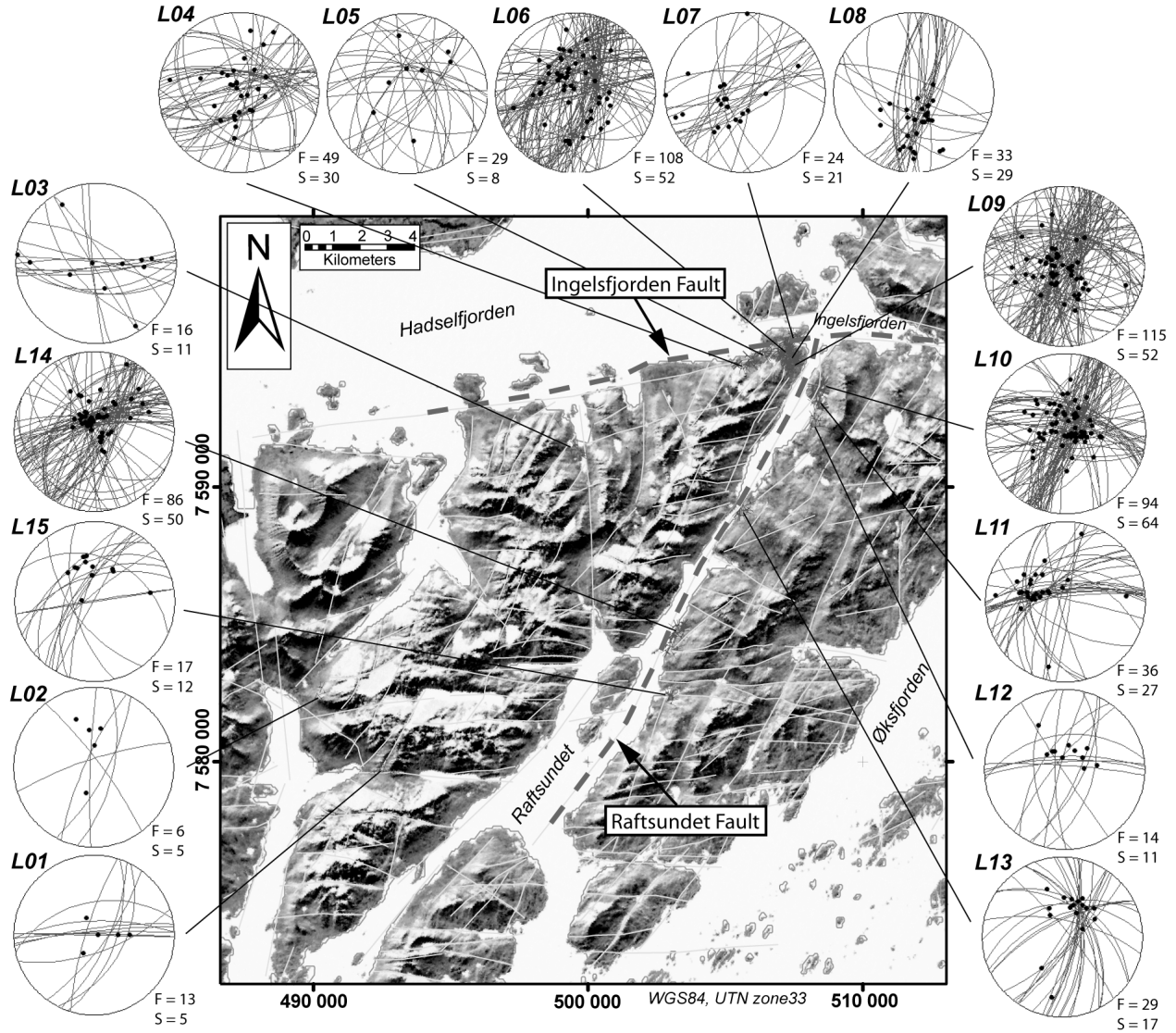


Figure 10. ArcGIS map showing location of fault populations and traverse sites, surrounded by individual stereonets for each locality. Stereonets plotted using GIS Stereoplot [Knox-Robinson and Gardoll, 1998] for ArcView 3.x.

Table 1. Matrix of Age Relationships Between Faults (Based on Outcrop Observations) Constructed Using Methods of Potts and Reddy [1999]^a

Older	Younger					
	NE-SW (Oblique Slip)	ENE-WSW (Strike Slip)	ENE-WSW (Dip Slip)	NNE-SSW (Strike Slip)	NNE-SSW (Normal)	Low-Angle Normal Faults
NE-SW (oblique slip)		✓ (1)	✓ (3)	(not seen)	(not seen)	(not seen)
ENE-WSW (strike slip)	(not seen)		✓ (2)	✓ (2)	(not seen)	(not seen)
ENE-WSW (dip slip)	✓ (2)	✓ (4)		✓ (5)	✓ (4)	(not seen)
NNE-SSW (strike slip)	(not seen)	✓ (4)	✓ (1)		✓ (2)	✓ (1 - reactivated)
NNE-SSW (normal)	✓ (12)	(not seen)	✓ (5)	✓ (7)		(possible?)
Low-angle normal faults	✓ (2)	(not seen)	✓ (3)	✓ (5)	✓ (10)	

^aEach cell in the matrix represents a possible relative age for the six fault sets/movements identified. Note that relative ages are determined through crosscutting and overprinting (reactivation) relationships; however, kinematics and fault interaction are not taken into account. Values in parentheses refer to number of observations made.

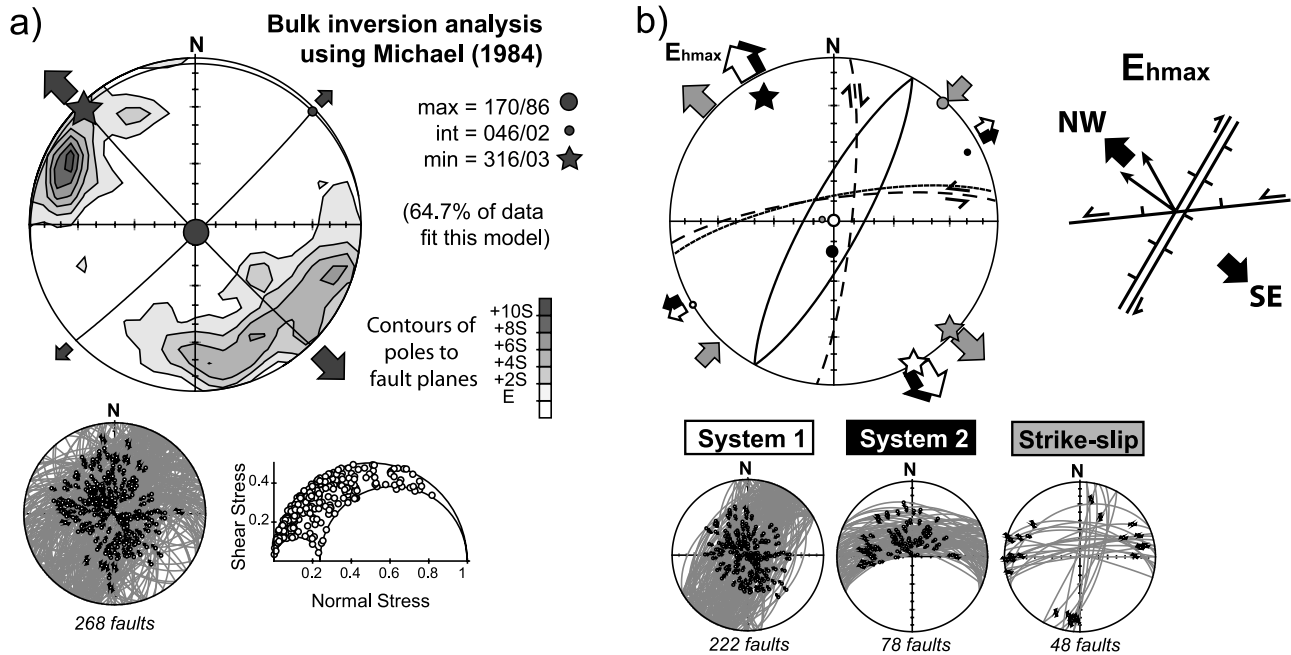


Figure 11. Kinematic inversion analysis. (a) Stereonet showing results of inversion analysis for bulk data (after 6 iterations) using *Michael's* [1984] method, plus stereonet of raw data and corresponding three-dimensional Mohr circle. (b) Stereonet showing results of inversion analysis for system 1 (dip slip) faults, system 2 (dip slip) faults, and strike-slip faults, using *Michael's* [1984] method. Arrows show horizontal stresses. All results suggest a NW-SE maximum horizontal extension (i.e., E_{hmax} range from 318° to 330°).

Ridge is a single, major, NNE-SSW trending fault with ~ 3 km throw (Figure 6a), whereas offshore north Lofoten the WLBF is much less prominent, and appears to bend round into a NE-SW or ENE-WSW trend (i.e., trend similar to the ridge) with a series of NNE-SSW trending, west dipping, splay faults, with lesser throw (Figure 6). There is also a change in fault polarity farther offshore, with east dipping normal faults appearing to accommodate much of the extensional strain seen farther south on the WLBF.

[57] Both onshore and offshore north Lofoten fault patterns appear complex; however, slight differences can be seen between these areas (i.e., compare stereonet in Figures 5 and 6). This is likely to be due to the onshore and offshore study areas being located on slightly different parts of the ridge (i.e., offshore data is from west of Vestvågøya and southern Austvågøya, whereas onshore data is from northern Austvågøya) and thus slightly different ridge trends (approximately ENE-WSW and approximately E-W, respectively). A further explanation may also be that onshore we are looking at deformation within basement rocks in the footwall to the border fault; while offshore it is deformation is within cover rocks of the hanging wall. However, onshore lineament trends on Vestvågøya appear similar to those offshore; therefore the former explanation appears more likely.

6.1.2. Regional Versus Field Measurements of Onshore Faults

[58] Regional fault models derived from lineament analysis for the NLD show a rhombic fault block pattern

(Figure 5), with the poles to planes of these regional faults clustering in a bimodal distribution (i.e., near vertical dips; Figure 5f). However, field observations suggest that many of these regional faults have a shallower dip than those suggested by our 3-D model. For example, Figure 7b shows 3 large fault traces identified in the field which dip at ~ 60 – 65° north. These faults were also recognized from lineaments on the Landsat image and in the GoCADTM model; however, these planes appear to dip at $>80^\circ$. Therefore it would appear that a limitation of this method of fitting best fit planes through lineament traces can lead to an over-steepening of the fault plane by ~ 10 – 15° . Hence any regional fault dipping at $>75^\circ$ is likely to appear near vertical in this model. Consequently, we interpret the derived lineament data as masking a multimodal fracture distribution which we relate to 3-D deformation, rather than 2-D plane strain (see below and *Oertel* [1965], *Reches* [1978], and *Krantz* [1989]).

6.2. Oblique Extension and Transtension in North Lofoten

6.2.1. Multimodal Faulting in North Lofoten: Polyphase Deformation or 3-D Strain?

[59] Rift systems that undergo extension oblique to the basin bounding faults commonly show complex multimodal fault patterns [e.g., *Withjack and Jamison*, 1986; *Clifton et al.*, 2000; *Dewey*, 2002; *De Paola et al.*, 2005a, 2005b]. As the extension directions calculated in north Lofoten appear moderately oblique to the trend of the ridge, it is likely that

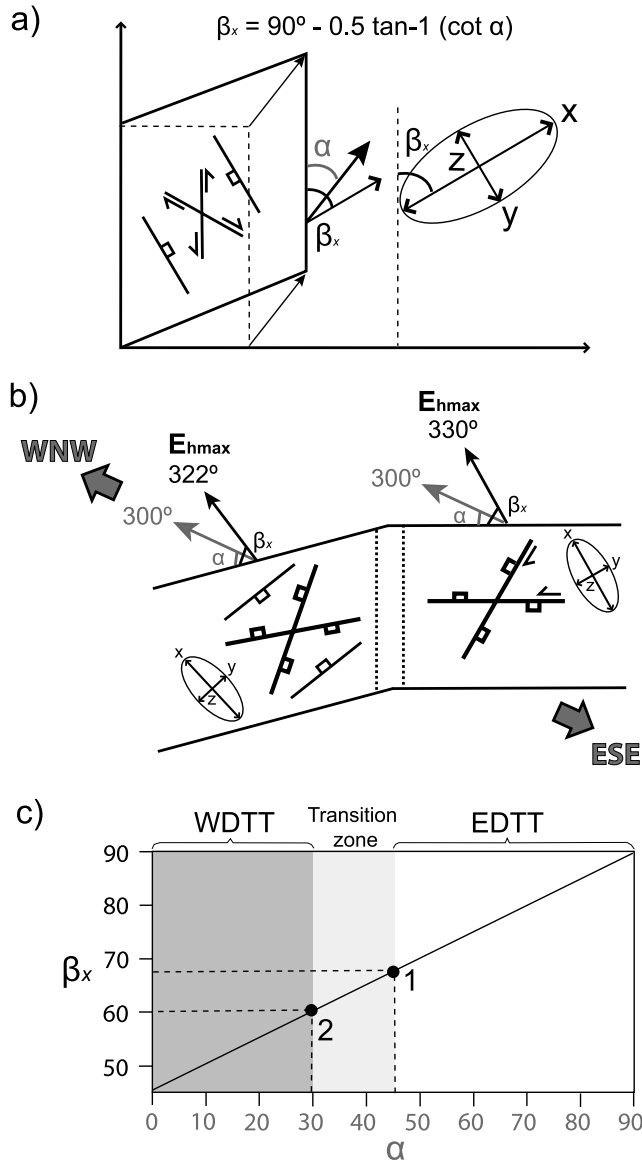


Figure 12. (a) Simplified box model summarizing relationship between α and β_x and the relative to the deformation boundary. (b) Cartoon diagram summarizing corrections due to obliquity between E_{hmax} and local ridge trend in order to estimate true regional extension (i.e., use equation (1) to calculate α (angle between regional extension vector and trend of ridge) from β_x (angle between E_{hmax} and trend of ridge)). (c) An α versus β_x plot corresponding to solution of equation (1) [from *De Paola et al., 2005a*]. Points 1 and 2 correspond to α and β_x angles for north Lofoten Ridge segments shown in Figure 12b. Results suggest fault patterns developed under oblique WNW-ESE extension.

this area has undergone transtensional deformation. Both regional and outcrop studies in north Lofoten have revealed an apparent multimodal fault geometry, i.e., fault patterns dominated by more than two distinct fault sets (Figure 8a). Multiple fault orientations are common in many geological

settings [e.g., *Krantz, 1988, 1989; Nieto-Samaniego and Alaniz-Alvarez, 1997; Sagy et al., 2003*]. *Nieto-Samaniego and Alaniz-Alvarez* [1997] proposed four main mechanisms to develop such multimodal fault patterns are (1) polyphase deformation (i.e., two or more sets of faults, developed due to two or more deformation events, assuming Andersonian fault models); (2) reactivation of noninteracting faults according to the *Bott* [1959] model; (3) faulting associated with 3-D strain (e.g., orthorhombic faulting [*Reches, 1978; Krantz, 1989*]); and (4) interacting block model [*Nieto-Samaniego and Alaniz-Alvarez, 1997*]. As transtensional deformation is a combination of extension and strike-slip deformation [*Sanderson and Marchini, 1984; Dewey, 2002*], fault patterns associated with 3-D strain are also likely to develop [*Reches, 1978; De Paola et al., 2005a*]. Therefore, during a bulk homogeneous transtensional deformation, case 3 seems to be the most likely kinematic solution which will govern the development of faulting patterns under infinitesimal strain fields. As finite strains accumulate, however, case 2 and particularly case 4 could increasingly become important [*Nieto-Samaniego and Alaniz-Alvarez, 1997; De Paola, 2005*]. This appears to be the case in north Lofoten where we see a regional set of multimodal faults not dissimilar to orthorhombic patterns of *Reches* [1978], with strong evidence for fault interaction in areas of highest fracture density (i.e., near major faults such as the Raftsundet Fault).

[60] An alternative model to transtension in north Lofoten is that each fault system developed independently (i.e., as suggested by S. G. Berge et al. (The Lofoten-Vesterålen continental margin: A multiphase Mesozoic-Palaeogene rifted shelf as shown by offshore-onshore brittle fracture analysis, submitted to *Norwegian Journal of Geology*, 2006, hereinafter referred to as Berge et al., submitted manuscript, 2006) during slightly different regional stress. Although some degree of polyphase deformation is apparent from observations made in this study (i.e., multiple slikenines and crosscutting relationships), mutual crosscutting relationships between S1 and S2 faults suggest they are likely to be contemporaneous. Thus we suggest that much of the apparent polyphase deformation seen in Lofoten is the result of fault interaction and localized variations in stress during a prolonged phase of deformation. This model is also favored by the fact that kinematic indicators on almost all faults correspond to a similar NW-SE extension. However, without better age constraints for individual fault movements, distinguishing which of these contrasting models is more likely is somewhat difficult.

6.2.2. Corrections Because of Oblique Extension

[61] Up to this point we have been discussing NW-SE extension axes based on observations in north Lofoten. However, in section 6.2.1 we suggest that the fault patterns in this area likely developed in transtension, and that maximum horizontal extension is oblique to the trend of the ridge. *Withjack and Jamison* [1986] show that during oblique rifting the orientation of maximum horizontal extension strain (E_{hmax}) is controlled by α , the angle between the rift trend and the direction of displacement. This is defined by the relationship between the angles α and

Table 2. Summary of the Predicted Orientations of Faults On the Basis of Fault Models of *Withjack and Jamison* [1986] for Segmented Transtension Model for the Lofoten Ridge^a

Deformation Zone (and Trend)	Deformation Type	α/β	Faults Predicted by <i>Withjack and Jamison</i> [1986]		
			Fault Type	Trend Relative to the Deformation Zone Boundary	Apparent Strain Axis
A (030)	pure extension	90/90	normal	0 (030)	290
B (075)	wrench/extension-dominated transtension	45/67	sinistral SS, dextral SS, normal	0°Counterclockwise (075), 60°Counterclockwise (015), 30°Counterclockwise (045)	322
C (090)	wrench-dominated transtension	30/60	sinistral SS, dextral SS	8°Counterclockwise (082), 68°Counterclockwise (012)	330

^aSee Figure 13. Regional extension is taken to be 300–120 (i.e., normal to mean trend of normal faults, which also matches results of applying equation (1) to mean “paleostress” vector determined through kinematic analysis in deformation zone C.

β , which correspond to the acute angles of the regional extension vector, and the maximum horizontal extension strain (E_{hmax}), respectively, measured relative to the deformation zone boundary (Figure 12a) according to (shown graphically in Figure 12c)

$$\beta_x = 90^\circ - 0.5 \tan^{-1}(\cot \alpha) \quad (1)$$

which may be rewritten more simply as [McCoss, 1986]

$$90^\circ - \beta_x = \frac{1}{2}(90^\circ - \alpha) \quad (2)$$

In north Lofoten, E_{hmax} (330° – 150°) inferred from lineament trends, and calculated from paleostress inversion, appears to be moderately oblique ($\beta_x \approx 60^\circ$) to the trend of the ridge (trend 090° – 270°). By applying equation (1), we see that this β_x angle corresponds to an α value of 30° , and thus implies a regional extension closer to WNW-ESE (300° ; Figure 12b and Table 2).

6.2.3. Orthogonal and Oblique Ridge Segments

[62] Ridge segment orientations relative to the direction of plate motion appear to play a critical role in determining the structural architecture of a particular ridge segment [see also *Taylor et al.*, 1994; *Clifton and Schlische*, 2003]. Onshore, variations in the dominant lineament/fracture trends along the Lofoten Ridge can be explained using a model for oblique extension/transtension along the LVA that develops due to the changing trend of the deforming zone boundary structures (i.e., border faults to the ridge) with respect to the regional extension vector (Figure 13). In this model there are three distinct deformation zones. In central Lofoten, there is a zone of orthogonal extension ($\alpha = 90^\circ$) (zone A), passing northward into two zones of transtension (B and C). Zone B corresponds to an angle α of $\sim 45^\circ$, which is close to the transition between extension-dominated and wrench-dominated transtension (shown as 20° in Figure 1, but it generally ranges from 30° to 40° for most rocks, Figure 12c; see *De Paola et al.* [2005a]) while zone C lies just within the wrench-dominated field (horizontal z axis) with an α value of 30° (Figure 13).

[63] The model for increasingly oblique transtension northward along the Lofoten Ridge is also consistent with offshore structural changes. Each zone is predicted to exhibit different faulting patterns and degrees of vertical shortening. In zone A, the shortening axis is vertical

predicting a significant amount of vertical thinning and rift-related subsidence. In zones B and C smaller amounts of vertical thinning and rift-related subsidence are predicted. Our observations offshore suggest that in the central Lofoten domain the WLBF has a large throw, with a deep sedimentary basin developed in its hanging wall. Along strike in the region offshore from the NLD, the fault throws are reduced and the basins are markedly shallower or even absent.

[64] In our model, the boundaries between each domain may have started off trending roughly N-S (perhaps controlled by preexisting Permian extensional structures (Figure 14) [*Steltenpohl et al.*, 2004]) and highly oblique to the regional extension. As extension continued these boundaries are likely to have rotated counterclockwise to lie parallel to the NNW-SSE trending transfer zones inferred by *Tsikalas et al.* [2001] (Figures 2 and 13).

6.2.4. Comparisons With Experimental Models and Other Field Analogues

[65] Experimental clay models for oblique rifting show that fault orientation will change with respect to the angle of obliquity, α (Figure 13c and Table 2) [*Withjack and Jamison*, 1986; *Clifton et al.*, 2000]. The fracture patterns predicted by these models show similar trends to those observed in lineament patterns for each domain along the Lofoten Ridge (Figure 3 and 13a). Significantly, the complex multimodal fault patterns and orientation of faults relative to the ridge bounding fault seen in north Lofoten (i.e., *Austvågøya* and *Vestvågøya*) resemble models for 20° – 30° oblique divergence (Figure 13c) [*Withjack and Jamison*, 1986; *Clifton et al.*, 2000]. This model for oblique extension also appears valid for offshore fault patterns which show an en echelon style set of faults splaying off the WLBF, and suggest a component of sinistral shear along the border fault (note that this may also explain the significant decrease in throw along the WLBF in this area). The kinematic inversion analysis of outcrop-scale faults within north Lofoten suggests a NW-SE extension. If we use the ridge trend in this domain (approximately E-W) to define regional-scale orientation of the deformation zone boundary faults, then $\beta = 60^\circ$ for the NLD. By applying equation (1), we obtain an angle $\alpha = 30^\circ$, and a regional extension vector (RE) oriented 300° (for exact values see Figure 12 and Table 2). Importantly, this WNW-ESE

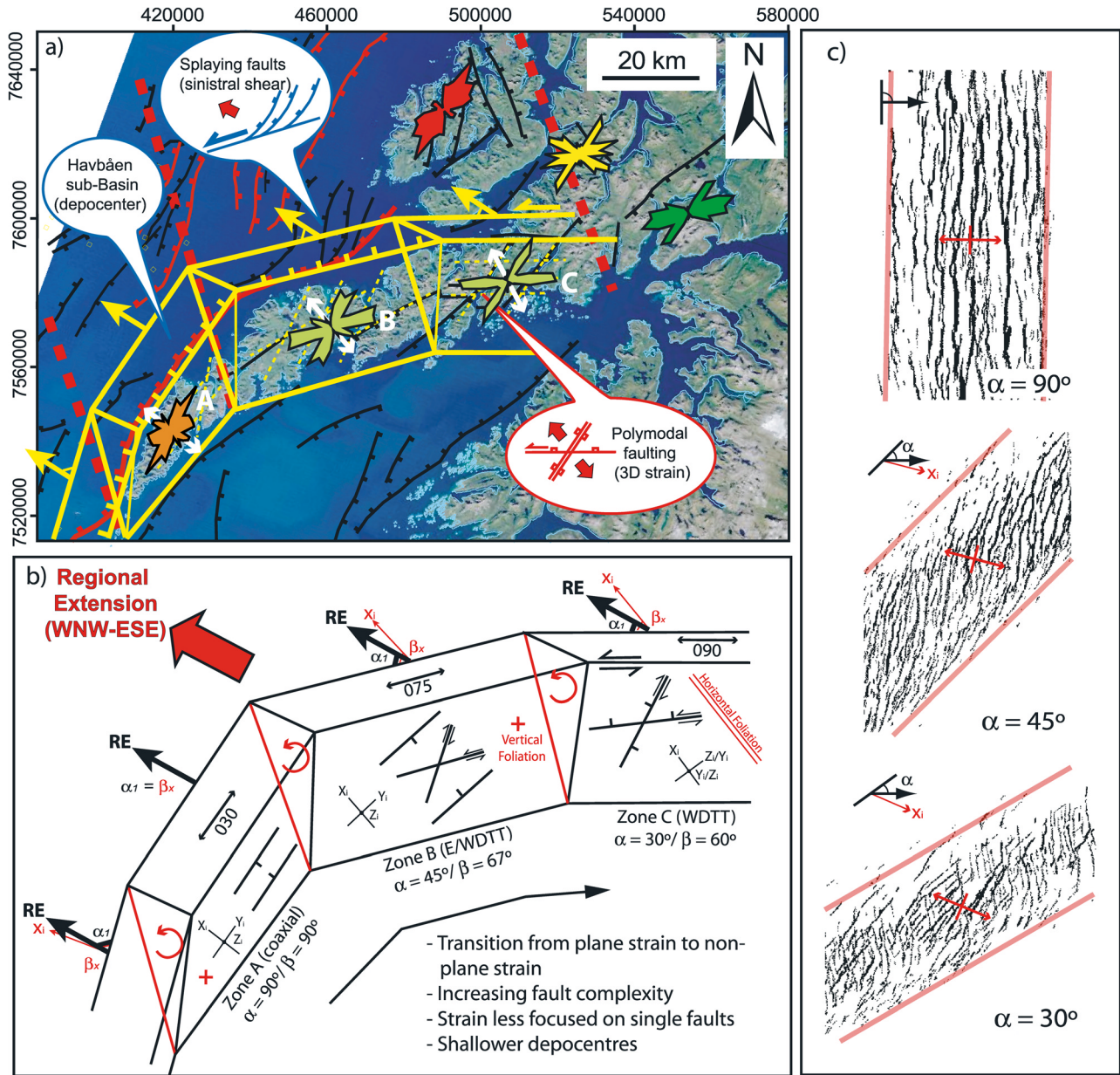


Figure 13. (a) Summary map showing variations in fault patterns and structural style along the Lofoten Ridge. A, B, C refer to deformation zones described in Table 2. Rose diagrams show summary of lineament trends for each lineament domain outlined in Figure 3. Offshore faults adapted from *Tsikalas et al.* [2001]. (b) Predicted deformation patterns and the effects of increasing obliquity along the Lofoten Ridge (based on models of *Withjack and Jamison* [1986] and *Dewey* [2002]) (see also Table 2). (c) Fault trace maps for various angles of divergence, highlighting the effects of increasing obliquity (i.e., decreasing α) on fault patterns; taken from results of experimental clay models by *Clifton et al.* [2000].

extension direction corresponds well with extension directions documented along other parts of the Norwegian margin during the Early Cretaceous [e.g., *Mosar et al.*, 2002].

[66] Similar fault patterns to those seen in north Lofoten have also been observed on the Reykjanes Peninsula, SW Iceland, where plate motion is roughly 30° oblique to the plate boundary in a left lateral sense [*Taylor et al.*, 1994;

Clifton and Schlische, 2003]. In this example multimodal fault patterns are again apparent, with a combination of both strike-slip and dip-slip fault kinematics [*Clifton and Schlische*, 2003]. Recent studies have shown that these faults developed under a variable stress history, with alternating phases of extension-dominated and wrench-dominated deformation, over short geological timescales (i.e., less than 1000 years) [*Kattenhorn and Clifton*, 2005]. These

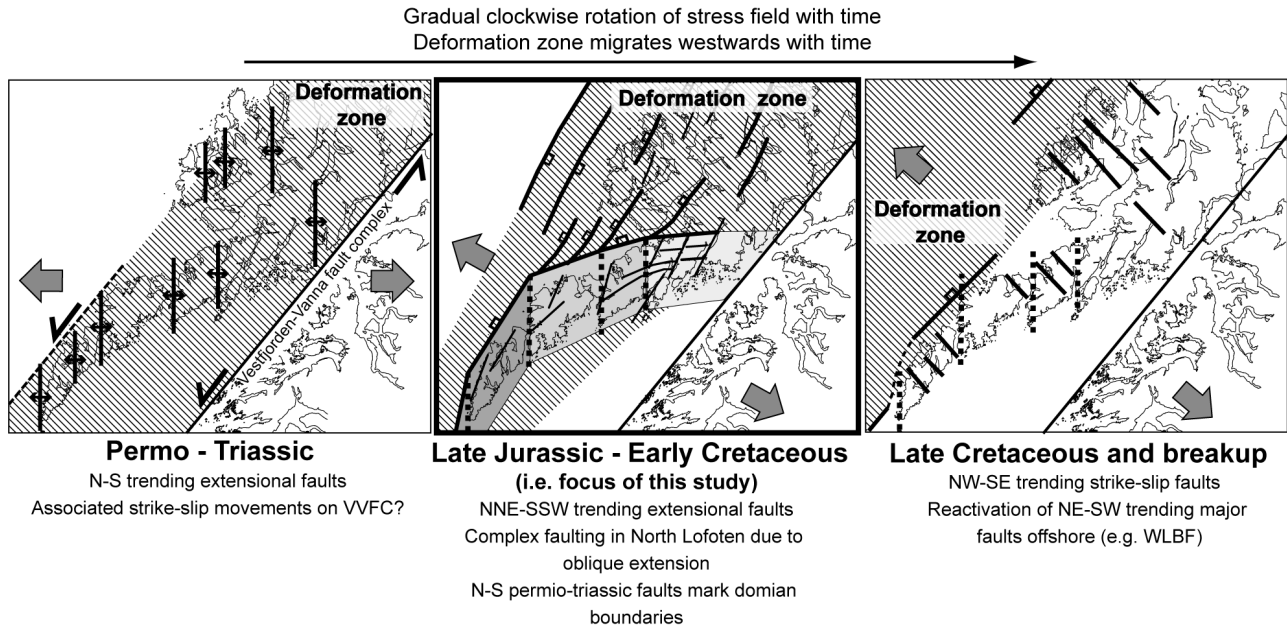


Figure 14. Possible model for the structural evolution of the Lofoten Ridge from Permian through to Eocene. Main structures discussed in this study correspond to Late Jurassic–Early Cretaceous extension.

variations in deformation style have been attributed to the influence of oscillatory magmatic events on local stress field, and have led to complex crosscutting, overprinting and fault reactivation, during what may be described as a single tectonic event [Holdsworth *et al.*, 1997]. A similar explanation may be applicable for the complex crosscutting relationships and overprinting of strike-slip and dip-slip slickenlines seen in the Lofoten as a relatively young Lamprophyre dike (compared to those described by Griffin *et al.* [1978]) was seen trending parallel to (084/82S), and reactivated by, system 2 faults (Figure 9a). A prominent set of tensile fractures/joints, were also seen trending parallel to this dike (Figure 7e). A second more highly deformed dike was also seen trending parallel to S1 faults (Figure 9b). The age of these dikes is unknown, but we suggest that they may have been emplaced synchronous with extensional faults and joint formation in these basement rocks (i.e., similar to the model of Kattenhorn and Clifton [2005]). However, as this model is based on the observation of just two Lamprophyre dikes, further field research is required.

[67] A further similarity between the observations made in this study and those described from the Reykjanes Ridge is the occurrence of complex fault interaction, particularly at the “inside corners” of fault/ridge segments [Clifton *et al.*, 2005]. As shown in Figure 9c, d a number of good examples of fault interaction have been observed in this study, all of which were found at the inside (i.e., footwall) corner between the intersecting Raftsundet and Ingelsfjorden Faults (i.e., localities LO6, LO8, and LO9; Figure 10).

6.3. Margin Segmentation and Evolution

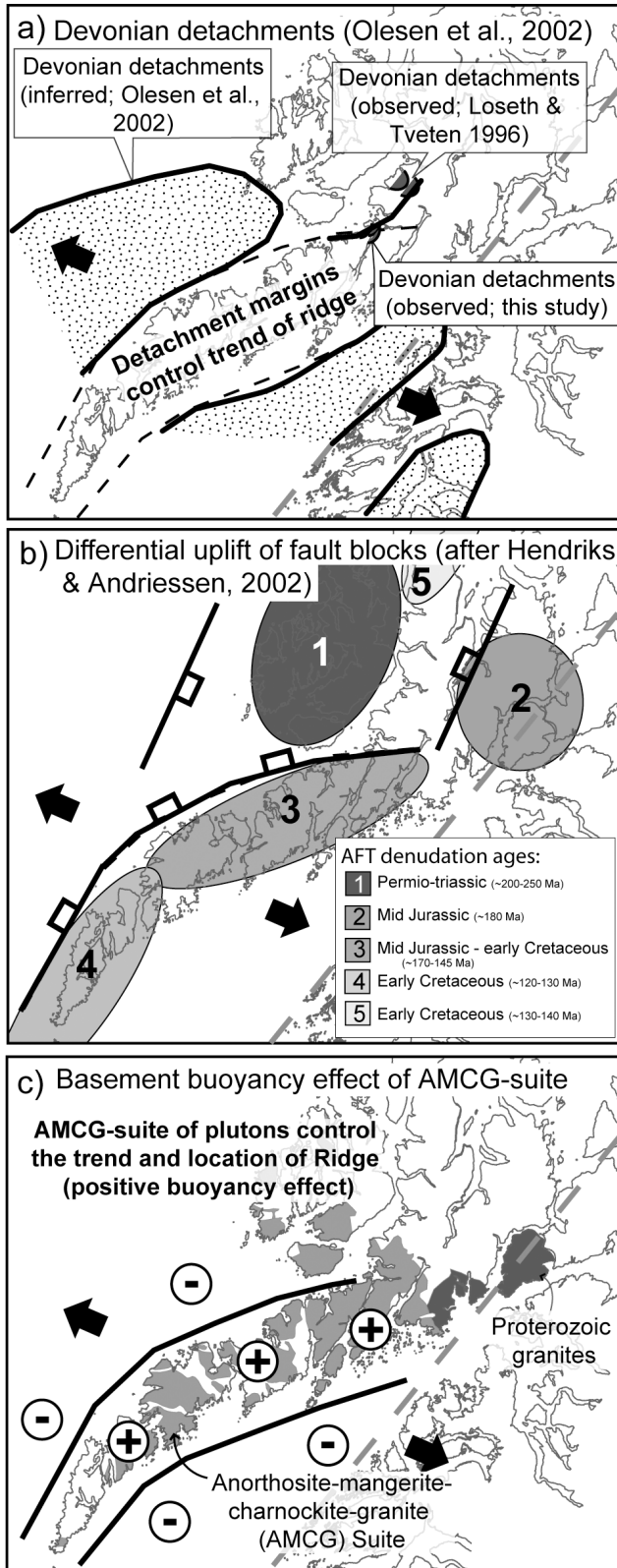
6.3.1. Ridge Development and Fault Evolution

[68] A number of different fault/fracture trends have been identified from lineament studies (S0–S3; Figures 3 and 4).

However, only two of these trends are accounted for in our model for oblique extension during the Late Jurassic and Early Cretaceous (i.e., S1 and S2). Age relationships interpreted from apparent crosscutting relationships identified during remote sensing and visualization of 2.5-D and 3-D models suggested that S0 lineaments are likely to be older and S3 lineaments younger, than S1/S2 structures. We therefore tentatively suggest a model for the development of these structures as follows: the progressive development of S0 faults/fractures during E-W extension, followed by S1/S2 faults developing during WNW-ESE oblique extension, and finally S3 strike-slip faults during NW-SE extension (Figure 14). Consistent with observations made by Lundin and Doré [1997] and Olesen *et al.* [1997] there is likely to have been a westward shift in deformation with time from the east Lofoten and the Vestafjorden-Vana fault complex during the Permian, through to offshore west Lofoten in the Cretaceous (Figure 14). This model is similar to the multistage model proposed by Berge *et al.* (submitted manuscript, 2006), the only exception being in our model S1 and S2 faults are active contemporaneously due to oblique extension. This suggested evolution is consistent with plate reconstructions of the Norwegian-Greenland margins which show E-W extension during Permian to Jurassic times, rotating progressively through WNW-ESE during Late Jurassic to Early Cretaceous, to NW-SE extension during Late Cretaceous and Paleogene, and ending with NW-SE seafloor spreading in the Eocene [Doré *et al.*, 1999; Mosar *et al.*, 2002].

6.3.2. Segmentation of the LVA: Transfer Zones and Segment Boundaries

[69] Most maps of both the Norwegian and Lofoten-Vesterålen margins show that they are segmented by a series of NW-SE transfer zones [Lundin and Doré, 1997;



Olesen et al., 1997, 2002; Brekke, 2000; Tsikalas et al., 2001]. This inferred segmentation of the Lofoten-Vesterålen region is based on changes in fault polarity and sediment thickness offshore, and crustal structure (derived from potential field data) onshore [Olesen et al., 1997, 2002; Tsikalas et al., 2001]. Hendriks and Andriessen [2002] have also shown that separate ridge segments appear to show different denudation histories. A number of rift segments and transfer zones have been proposed (see Figure 2), but there are disagreements concerning the exact position and orientation of these structures [e.g., Tsikalas et al., 2001; Olesen et al., 2002]. A key reason for this indecision on the location of these structures is the fact that no distinct lineaments representing these transfer zones can be identified.

[70] The Bivrost, Vesterålen and Senja transfer zones have been attributed to the influence of deep seated basement structures at depth [Olesen et al., 2002; Mjelde et al., 2003]. Known examples of such structures may include the Bothnian-Kvænangen and the Bothnian-Senja fault complexes (Figure 2). It is somewhat difficult, however, to link other transfer zones on the LVA (e.g., the Mosken, Jennegga transfer zones) to such basement shear zones. Instead, these transfer zone boundaries appear to be zones of “soft linkage” (or accommodation zones [Peacock et al., 2000]) between margin segments characterized by different basin and fault geometries. Furthermore, the structure of these differing margin segments appears to correspond to variations in the divergence angle between the ridge (or margin) bounding faults and the regional extension vector (Figure 13). Similar observations have also been made along the Brazilian margin of the South Atlantic [Davison, 1997] where the width of the margin may also be linked to obliquity.

6.3.3. Origins of Oblique Ridge Segments

[71] As our model for margin segmentation is based on the influence of oblique margin segments, we must therefore assess the origins of margin obliquity. Oblique extension is generally associated with the reactivation or control of preexisting structures [Holdsworth et al., 1997]. No distinct fabrics (e.g., shear zones, strong foliation, etc.)

Figure 15. Possible controls on the development of the obliquely trending north Lofoten Ridge segment. (a) Reactivation of “spoon-shaped” Devonian detachment faults that may have controlled the trend of the northern part of the Lofoten Ridge [Olesen et al., 2002]. However, only localized reactivation of Devonian low-angle faults has been observed in this study. (b) Differential uplift of fault blocks from Permian to Cretaceous that may effect the development of fault trends in neighboring blocks (i.e., older fault blocks in result in outer Vesterålen Block, block 1, may have acted as a barrier to later faults developing during the uplift of the main Lofoten Ridge, blocks 2, 3, and 4). Denudation ages from AFT studies by Hendriks [2003]. (c) A basement buoyancy effect caused by the AMCG suite (anorthosite-mangerite-charnockite-granite) underlying much of North Lofoten that may have led to the preferential uplift of an oblique trending ridge block, i.e., similar to effect of granites under Mid-North Sea High [Donato et al., 1983].

were observed within the basement rocks studied that could directly account for the oblique trend of the north Lofoten Ridge. A few discreet E-W trending joints and dikes were recorded that appear to be reactivated by faults at outcrop; however, the age of these is unclear (i.e., they may be synchronous with faulting), and they are not intense enough to account for the overall change in ridge trend. Figure 15 shows three possible origins for this obliquity; however, research is required to investigate these further.

[72] *Olesen et al.* [2002] proposed a model in which the border faults to the north Lofoten Ridge reactivate “spoon-shaped” Devonian detachments (Figure 15a; also see Figure 16 of *Olesen et al.* [2002]). Field observations of these low-angle, Devonian, detachment structures have been made in Hinnøya [*Løseth and Tveten*, 1996] and northern Austvågøya (this study). However, such low-angle structures are only likely to have a limited effect on the location and orientation of steeply dipping Mesozoic basin bounding extensional structures, and therefore further structural influence is required. Geophysical studies [*Sellevoll*, 1983; *Olesen et al.*, 1997, 2002] in central and northern Norway show the Lofoten Ridge to be associated with strong magnetic and gravimetric anomalies. A positive gravity anomaly beneath the south and central Lofoten Ridge are believed to reflect a shallow Moho discontinuity and uplifted high-grade rocks of intermediate density [*Sellevoll*, 1983; *Olesen et al.*, 2002]. This exhumation of rocks from the deep crust has led some authors to describe Lofoten as a “core complex” [*Hames and Anderson*, 1996] which may have developed as far back as the Devonian.

[73] Recent Apatite fission track (AFT) studies suggest that the LVA has undergone differential block uplift in post-Caledonian times (Figure 15b). *Hendriks and Andriessen* [2002] document various AFT ages along the LVA indicating differential vertical movements across the area. The oldest cooling/denudation ages were observed on Langøya, which indicate uplift/exhumation during the Permian/Triassic. North Lofoten on the other hand shows evidence for cooling/denudation from Mid-Jurassic to Early Cretaceous. It is possible that the earlier exhumed Langøya block acted as a barrier to the developing WLBF, thus leading to it deflecting eastward toward the already established Vestfjorden-Vanna fault complex [*Olesen et al.*, 1997]. As the WLBF changes in trend, strain is also accommodated by east dipping faults farther offshore, and to the west of the Langøya Block, thus leading to a Jurassic/Cretaceous basin bound on three sides on Vesterålen (Figure 15b) [*Dalland*, 1981; *Daividsen et al.*, 2001].

[74] A third model is one of basement buoyancy similar to the models proposed by *Bott* [1967] and *Donato et al.* [1983] for parts of the North Sea. The rocks of the north Lofoten Ridge are dominated by an anorthosite-mangerite-charnockite-granite (AMCG) suite of plutons (Figure 15c) [*Griffin et al.*, 1978; *Corfu*, 2004a] dating from ~ 1.8 Ga. The basement rocks on south Lofoten on the other hand are dominantly older Archaean/Paleoproterozoic gneisses [*Tveten*, 1978; *Corfu*, 2004a]. These granites typically have a slightly lower density than the surrounding basement rocks, which may lead to a slight buoyancy effect of the

granites as they move toward equilibrium with the surrounding basement [*Bott*, 1967]. This basement buoyancy effect has been used to explain the tectonic stability and/or uplift of areas underlain by granites [*Bott*, 1967; *Donato et al.*, 1983]. In addition, it has been suggested that this stability is most effective during times of extension [*Bott et al.*, 1978]. It is possible that the AMCG suite may have controlled the trend and development of the north Lofoten Ridge in this manner (Figure 15c). However, as these granites are of Precambrian age, it is likely that they reached equilibrium with surrounding rocks long before the Cretaceous, although it is possible that this buoyancy effect may have influenced the development of the Devonian detachments described above [*Olesen et al.*, 2002]. This may also explain the apparent elevated nature of the Lofoten Ridge through time [*Sherlock*, 2001]. Although each of the models presented in Figure 15 are presented as mutually exclusive hypotheses, they may all play a role in the development of the ridge and could be applicable in combination.

7. Conclusions and Implications for Future Exploration on the Norwegian Margin

[75] Through an integrated onshore, offshore and regional to outcrop-scale fault study we present a self-consistent structural model for transtension and structural segmentation along the Lofoten Ridge. Segment orientations relative to the direction of regional extension appear to play a critical role in determining the structural architecture of each particular ridge segment [see also *Taylor et al.*, 1994; *Clifton and Schlische*, 2003].

[76] The Lofoten-Vesterålen archipelago can be divided into a series of distinct structural domains reflecting varying fault patterns. These domains are concurrent with changes in trend of the Lofoten Ridge; therefore we attribute these variations in fault/fracture pattern to changes in α (the angle between the trend of the ridge and the regional extension vector; Figures 1, 12, and 13). Analysis of lineament trends and kinematic analysis of field data (including paleostress inversion) suggest a maximum horizontal extension (E_{hmax}) direction of $\sim 320^\circ$ to 325° in north Lofoten. This corresponds to a β_x value of $\sim 60^\circ$ and thus an α of $\sim 30^\circ$. Therefore regional extension associated with this deformation is WNW-ESE. This model for oblique extension is supported by offshore variations depocenter location and fault geometry, with deep basins and simple faulting typical of areas where the ridge/border fault is orthogonal to extension, and complex faulting and less subsidence in more oblique settings. The changes in fault orientation, fault geometry and inferred extension directions for each domain in the Lofoten are consistent with analogue studies and experimental clay models of where the boundary conditions become increasingly oblique to extension (Figure 12) [*Withjack and Jamison*, 1986; *Clifton et al.*, 2000; *Clifton and Schlische*, 2003; *Dewey*, 2002].

[77] No major basement structures (e.g., shear zones) have been identified either onshore or offshore separating segment domains, and are thus instead interpreted as zones of soft linkage or accommodation zones. Therefore previ-

ously identified transfer zones segmenting the Lofoten Ridge, such as the Mosken and Jennegga transfer zones (Figure 2) [Tsikalas et al., 2001] may thus be attributed to changes in deformation style between margin segments of differing obliquity (i.e., second-order transfer zones) rather than reactivation of basement structures as proposed for other transfer zones on the margin (e.g., Bivrost and Vesterålen transfer zones; first-order transfer zones).

[78] Our results highlight that zones of oblique extension generally exhibit complex fault patterns characteristic of 3-D strain, and also less localized deformation compared to areas of orthogonal extension. These variations in structural style and depocenter location seen along the Lofoten Ridge may have important implications when assessing the likelihood of hydrocarbon plays and reservoir potential along other orthogonal and oblique rift segments of the Norwegian, and other, passive margins (e.g., Nordland Ridge, Utrøst Ridge and Gjallar Ridge [Mosar, 2003]). A number of recent studies of basement ridge structures on the Norwegian margin have shown that ridge trend relative to the regional sortening/extension vector plays an important role in the complexity of basins and potential reservoir plays [e.g., Gernigon et al., 2003;

Ren et al., 2003; Imber et al., 2005]. Many of these studies attribute these complex reservoirs to later reactivation of rift systems [e.g., Imber et al., 2005]. Our study broadly confirms this suggestion and additionally illustrates that these zones of complexity can form early in the development of rifted margin due to variations in initial rift trend that may be themselves controlled by features originating in the deeper basement.

[79] **Acknowledgments.** This paper has resulted from a NERC Ocean Margins LINK project (NER/T/S/2000/01018) cofunded by BP and Statoil (UK) Ltd. and associated tied studentship (NER/S/S/2001/06740). The fieldwork carried out in this paper was funded by an AAPG grants-in-aid award and by the Geological Society's Annie Greenly fund for detailed geological mapping. C. Morley, M. Daignieres, and an anonymous reviewer are thanked for their reviews and comments that helped to improve this paper significantly. Thanks to Schlumberger and Badley Geoscience Ltd. for kindly providing seismic interpretation software (GeoFrame[®] and Trapt Tester) and T. Henningsen for releasing the seismic data used in this study. R.W.W. would like to thank B. Hendriks, J. Dehls, N. De Paola, and P. Clegg for their help and advice at various stages of this study and to S. Berge for his discussions and debate on the development of faults in Lofoten. The authors would also like to thank A. Doré for his continued support and encouragement to the Reactivation Research Group at Durham.

References

- Andresen, A., and T. Forslund (1987), Post-Caledonian brittle faults in Troms: Geometry, age and tectonic significance, paper presented at the Caledonian and Related Geology of Scandinavia Conference, Dep. of Geol., Univ. Coll., Cardiff, U.K., 22–23 Sept.
- Angelier, J. (1984), Tectonic stress analysis of fault slip data sets, *J. Geophys. Res.*, *89*, 5835–5848.
- Angelier, J. (1994), Fault slip analysis and palaeostress reconstruction, in *Continental Deformation*, edited by P. L. Hancock, pp. 53–101, Elsevier, New York.
- Bartley, J. M. (1982), Limited basement involvement in Caledonian deformation, Hinna, north Norway, and tectonic implications, *Tectonophysics*, *83*, 185–203.
- Blystad, P., H. Brekke, R. B. Færseth, B. T. Larsen, J. Skogseid, and B. Torudbakken (1995), Structural elements of the Norwegian continental shelf II: The Norwegian Sea region, *NPD Bull.* *8*, Norw. Pet. Dir., Stavanger.
- Bosworth, W., G. S. Lister, M. A. Etheridge, and P. A. Symonds (1986), Comment and reply on 'Detachment faulting and the evolution of passive continental margins', *Geology*, *14*, 890–892.
- Bott, M. H. P. (1959), The mechanics of oblique slip faulting, *Geol. Mag.*, *96*, 109–117.
- Bott, M. H. P. (1967), Geophysical investigations of the northern Pennine basement rocks, *Proc. Yorkshire Geol. Soc.*, *36*, 139–168.
- Bott, M. H. P., J. Robinson, and M. M. Kohnstamm (1978), Granite beneath Market Weighton, east Yorkshire, *J. Geol. Soc. London*, *135*, 535–543.
- Brekke, H. (2000), The tectonic evolution of the Norwegian Sea continental margin with emphasis on the Vøring and Møre basins, in *Dynamics of the Norwegian Margin*, edited by A. Nøttvedt, *Geol. Soc. Spec. Publ.*, *167*, 327–378.
- Cashman, P. H., and M. A. Ellis (1994), Fault interaction may generate multiple slip vectors on a single fault surface, *Geology*, *22*, 1123–1126.
- Clegg, P., I. Trinks, K. J. W. McCaffrey, R. E. Holdsworth, R. R. Jones, R. Hobbs, and S. Waggott (2005), Towards the virtual outcrop, *Geoscientist*, *15*(1), 8–9.
- Clemson, J., J. Cartwright, and J. Booth (1997), Structural segmentation and the influence of basement structure on the Namibian passive margin, *J. Geol. Soc. London*, *154*, 477–482.
- Clifton, A. E., and R. W. Schlische (2003), Fracture populations on the Reykjanes Peninsula, Iceland: Comparison with experimental clay models of oblique rifting, *J. Geophys. Res.*, *108*(B2), 2074, doi:10.1029/2001JB000635.
- Clifton, A. E., R. W. Schlische, M. O. Withjack, and R. V. Ackermann (2000), Influence on rift obliquity on fault-population systematics: Results of experimental clay models, *J. Struct. Geol.*, *22*, 1491–1509.
- Clifton, A. E., S. A. Kattenhorn, and L. Fernandes (2005), Structural architecture of a highly oblique divergent plate boundary, *Geophys. Res. Abstr.*, *7*, Abstract 03398.
- Colletta, B., P. Le Quellec, J. Letouzey, and I. Moretti (1988), Longitudinal evolution of the Suez rift structure (Egypt), *Tectonophysics*, *153*, 221–233.
- Corfu, F. (2004a), U-Pb age, setting and tectonic significance of the Anorthosite-Mangerite-Charnockite-Granite Suite, Lofoten-Vesterålen, Norway, *J. Petrol.*, *45*, 1799–1819.
- Corfu, F. (2004b), U-Pb geochronology of the Leknes Group: An exotic Early Caledonian metasedimentary assemblage stranded on Lofoten basement, northern Norway, *J. Geol. Soc. London*, *161*, 619–629.
- Dalland, A. (1981), Mesozoic sedimentary succession at Andøy, northern Norway, and relation to the structural development of the North Atlantic area, *Can. Soc. Pet. Geol. Mem.*, *7*, 563–584.
- Davidsen, B., M. Smelror, and D. Ottesen (2001), Et nyoppdaget Mesozoisk basseng i Sortlandsundet, Vesterålen, in *XVII Vinterkonferanse, Abstracts Volume*, pp. 42–43, Norsk Geol. Forening, Trondheim, Norway.
- Davison, I. (1997), Wide and narrow margins of the Brazilian South Atlantic, *J. Geol. Soc. London*, *154*, 471–476.
- Delvaux, D., and B. Sperner (2003), New aspects of tectonic stress inversion with reference to the TENSOR program, in *New Insights Into Structural Interpretation and Modelling*, edited by D. A. Nieuwland, *Geol. Soc. Spec. Publ.*, *212*, 75–100.
- De Paola, N. (2005), The structural evolution of transtensional basins and rifted margin, Ph.D. thesis, Univ. of Durham, Durham, U. K.
- De Paola, N., R. E. Holdsworth, and K. J. W. McCaffrey (2005a), The influence of lithology and pre-existing structures on reservoir-scale faulting patterns in transtensional rift zones, *J. Geol. Soc. London*, *162*, 471–480.
- De Paola, N., R. E. Holdsworth, K. J. W. McCaffrey, and M. R. Barchi (2005b), Partitioned transtension: An alternative to basin inversion models, *J. Struct. Geol.*, *27*, 607–625.
- Dewey, J. F. (2002), Transtension in arcs and orogens, *Int. Geol. Rev.*, *44*, 402–439.
- Donato, J. A., W. Martindale, and M. C. Tully (1983), Buried granites within the mid North Sea High, *J. Geol. Soc. London*, *140*, 825–837.
- Doré, A. G., E. R. Lundin, C. Fichler, and O. Olesen (1997), Patterns of basement structure and reactivation along the NE Atlantic margin, *J. Geol. Soc. London*, *154*, 85–92.
- Doré, A. G., E. R. Lundin, L. N. Jensen, Ø. Birkeland, P. E. Eliassen, and C. Fichler (1999), Principal tectonic events in the evolution of the northwest European Atlantic margin, in *Petroleum Geology of Northwest Europe: Proceedings of the Fifth Conference*, edited by A. J. Fleet and S. A. R. Boldy, pp. 41–61, Geol. Soc. London, London.
- Edmondo, G. P. (2002), Digital geologic field mapping using ArcPad, digital mapping techniques 2002, workshop proceedings, *U.S. Geol. Surv. Open File Rep.*, *02-370*, 129–134.
- Eide, E. A. (Coord.) (2002), BATLAS—Mid Norway plate reconstruction atlas with global and Atlantic perspectives, 75 pp., Geol. Surv. of Norw., Oslo.
- Eldholm, O., E. Sundvor, and A. Myhre (1979), Continental margin off Lofoten-Vesterålen, northern Norway, *Mar. Geophys. Res.*, *4*, 3–35.

- Eldholm, O., J. Thiede, and E. Taylor (1989), Evolution of the Vøring volcanic margin, *Proc. Ocean Drill. Program Sci. Results*, 104, 1033–1065.
- Etchecopar, A., G. Vasseur, and M. Daignieres (1981), An inverse problem in microtectonics for the determination of stress tensors from fault striation analysis, *J. Struct. Geol.*, 3, 51–65.
- Fichler, C., E. Rundhovde, O. Olesen, B. M. Sæther, H. Rueslåtten, E. R. Lundin, and A. G. Doré (1999), Regional tectonic interpretation of image enhanced gravity and magnetic data covering the mid-Norwegian Shelf and adjacent mainland, *Tectonophysics*, 306, 183–197.
- Fossen, H. (2000), Extensional tectonics in the Caledonides: Synorogenic or postorogenic?, *Tectonics*, 19, 213–224.
- Fossen, H., and W. J. Dunlap (1998), Timing and kinematics of Caledonian thrusting and extensional collapse, southern Norway: Evidence from $^{40}\text{Ar}/^{39}\text{Ar}$ thermochronology, *J. Struct. Geol.*, 20, 765–781.
- Francheteau, J., and X. Le Pichon (1972), Marginal fracture zones as structural framework of continental margins in South Atlantic Ocean, *AAPG Bull.*, 56, 991–1007.
- Gabrielsen, R. H., and I. B. Ramberg (1979), Fracture patterns in Norway from Landsat imagery: Results and potential use, in *Proceedings of the Norwegian Sea Symposium*, pp. 1–28, Norw. Pet. Soc., Tromsø, Norway.
- Gabrielsen, R. H. A. Braathen, J. Dehls, and D. Roberts (2002), Tectonic lineaments of Norway, *Norw. J. Geol.*, 82, 153–174.
- Gernigon, L., J. C. Ringenbach, S. Planke, B. Le Gall, and H. Jonquet-Kolstø (2003), Extension, crustal structure and magmatism at the outer Vøring Basin, Norwegian margin, *J. Geol. Soc. London*, 160, 197–208.
- Gibbs, A. D. (1984), Structural evolution of extensional basin margins, *J. Geol. Soc. London*, 141, 609–620.
- Griffin, W. L., P. N. Taylor, J. W. Hakkinen, K. S. Heier, I. K. Iden, E. J. Krogh, O. Malm, K. I. Olsen, D. E. Ormaasen, and E. Tveten (1978), Archaean and Proterozoic crustal evolution in Lofoten-Vesterålen, N Norway, *J. Geol. Soc. London*, 135, 629–647.
- Hames, W. E., and A. Anderson (1996), Timing of Palaeozoic orogeny and extension in the continental shelf of north-central Norway as indicated by laser $^{40}\text{Ar}/^{39}\text{Ar}$ muscovite dating, *Geology*, 24, 1005–1008.
- Heier, K. S. (1960), Petrology and geochemistry of high-grade metamorphic and igneous rocks on Langøya, northern Norway, *Norg. Geol. Undersøkelse*, 207, 246 pp.
- Hendriks, B. W. H. (2003), Cooling and denudation of the Norwegian and Barents Sea Margin, northern Scandinavia, Ph.D. thesis, 177 pp., Vrije Univ., Amsterdam.
- Hendriks, B. W. H., and P. A. M. Andriessen (2002), Pattern and timing of the post-Caledonian denudation of northern Scandinavia constrained by apatite fission-track thermochronology, in *Exhumation of the North Atlantic Margin: Timing, Mechanisms and Implications for Petroleum Exploration*, edited by A. G. Doré et al., *Geol. Soc. Spec. Publ.*, 196, 117–137.
- Henkel, H. (1991), Magnetic crustal structures in northern Fennoscandia, *Tectonophysics*, 192, 57–79.
- Hodgetts, D., N. J. Drinkwater, J. Hodgson, J. Kavanagh, S. S. Flint, K. J. Keogh, and J. A. Howell (2004), Three dimensional geological models from outcrop data using digital data collection techniques: An example from the Tanqua Karoo depocenter, South Africa, in *Geological Prior Information*, edited by A. Curtis and R. Wood, *Geol. Soc. Spec. Publ.*, 239, 57–75.
- Hodgson, R. A. (1961), Classification of structures on joint surfaces, *Am. J. Sci.*, 259, 493–502.
- Holdsworth, R. E. C. A. Butler, and A. M. Roberts (1997), The recognition of reactivation during continental deformation, *J. Geol. Soc. London*, 154, 73–78.
- Imber, J., R. E. Holdsworth, K. J. W. McCaffrey, R. W. Wilson, R. R. Jones, R. W. England, and G. Gjeldvik (2005), Early Tertiary sinistral transpression and fault reactivation in the western Vøring Basin, Norwegian Sea: Implications for hydrocarbon exploration and pre-break-up deformation in ocean margin basins, *AAPG Bull.*, 89, 1043–1069.
- Jones, R. R., K. J. W. McCaffrey, R. W. Wilson, and R. E. Holdsworth (2004), Digital field data acquisition: Towards increased quantification of uncertainty during geological mapping, in *Geological Prior Information*, edited by A. Curtis and R. Wood, *Geol. Soc. Spec. Publ.*, 239, 43–56.
- Karpuz, M. R., D. Roberts, O. Olesen, R. H. Gabrielsen, and T. Herrevold (1993), Application of multiple data sets to structural studies on Varanger Peninsula, northern Norway, *Int. J. Remote Sens.*, 14, 979–1003.
- Karpuz, M. R., D. Roberts, V. M. Moralev, and E. Terekhov (1995), Regional lineaments of eastern Finnmark, Norway, and the western Kola Peninsula, Russia, *Norg. Geol. Undersøkelse Spec. Publ.*, 7, 121–135.
- Kattenhorn, S. A., and A. E. Clifton (2005), Time-variable faulting behaviour at an oblique spreading centre, southwest Iceland, *Geol. Soc. Am. Abstr. Programs*, 37(7), 421.
- Klein, A. C., and M. G. Steltenpohl (1999), Basement-cover relations and late- to post-Caledonian extension in the Leknes group, west-central Vestvågøy, Lofoten, north Norway, *Nor. Geol. Tidsskr.*, 79, 19–31.
- Knox-Robinson, C. M., and S. J. Gardoll (1998), GIS-stereonet: An interactive stereonet plotting module for ArcView 3.0 geographic information system, *Comput. Geosci.*, 24, 243–250.
- Krantz, R. W. (1988), Multiple fault sets and three-dimensional strain: Theory and application, *J. Struct. Geol.*, 10, 225–237.
- Krantz, R. W. (1989), Orthorhombic fault patterns: The odd axis model and slip vector orientations, *Tectonics*, 8, 483–495.
- Lister, G. S., M. A. Etheridge, and P. A. Symonds (1991), Detachment models for the formation of passive continental margins, *Tectonics*, 10, 1038–1064.
- Longley, P. A., M. F. Goodchild, D. J. Maguire, and D. W. Rhind (2001), *Geographic Information Systems and Science*, 454 pp., John Wiley, Hoboken, N. J.
- Løseth, T., and E. Tveten (1996), Post-Caledonian structural evolution of the Lofoten and Vesterålen offshore and onshore areas, *Nor. Geol. Tidsskr.*, 76, 215–230.
- Lundin, E. R., and A. G. Doré (1997), A tectonic model for the Norwegian passive margin with implications for the NE Atlantic: Early Cretaceous to break-up, *J. Geol. Soc. London*, 154, 545–550.
- Maerten, L. (2000), Variation in slip on intersecting normal faults: Implications for palaeostress inversion, *J. Geophys. Res.*, 105, 25,553–25,565.
- Maerten, L., D. D. Pollard, and F. Maerten (2001), Digital mapping of three-dimensional structures of the Chimney Rock fault system, central Utah, *J. Struct. Geol.*, 23, 585–592.
- McCaffrey, K. J. W., R. R. Jones, R. E. Holdsworth, R. W. Wilson, P. Clegg, J. Imber, N. Holliman, and I. Trinks (2005), Unlocking the spatial dimension: Digital technologies and the future of geoscience fieldwork, *J. Geol. Soc. London*, 162, 927–938.
- McClay, K. R., T. Dooley, P. Whitehouse, and M. Mills (2002), 4D evolution of rift systems: Insights from scaled physical models, *AAPG Bull.*, 86, 935–959.
- McCoss, A. M. (1986), Simple constructions for deformation in transpression/transension zones, *J. Struct. Geol.*, 8, 715–718.
- Michael, A. J. (1984), Determination of stress from slip data: Faults and folds, *J. Geophys. Res.*, 89, 11,517–11,526.
- Mjelde, R., H. Shimamura, T. Kanazawa, S. Kodaira, T. Raum, and H. Shiobara (2003), Crustal lineaments, distribution of lower crustal intrusives and structural evolution of the Vøring Margin, NE Atlantic: New insight from wide-angle seismic models, *Tectonophysics*, 369, 199–218.
- Mokhtari, M., and R. Pegrum (1992), Structure and evolution of the Lofoten continental margin, offshore Norway, *Nor. Geol. Tidsskr.*, 72, 339–355.
- Morley, C. K., R. A. Nelson, T. L. Patton, and S. G. Munn (1990), Transfer zones in the East African Rift system and their relevance to hydrocarbon exploration in rifts, *AAPG Bull.*, 74, 1234–1253.
- Morley, C. K., C. Haranya, W. Phoosongsee, S. Pongwapee, A. Komsawan, and N. Wonganan (2004), Activation of rift oblique and parallel pre-existing fabrics during extension and their effect on deformation style: Examples from the rift of Thailand, *J. Struct. Geol.*, 26, 1803–1829.
- Mosar, J. (2003), Scandinavia's North Atlantic passive margin, *J. Geophys. Res.*, 108(B8), 2360, doi:10.1029/2002JB002134.
- Mosar, J., E. A. Eide, P. T. Osmundsen, A. Sommaruga, and T. H. Torsvik (2002), Greenland-Norway separation: A geodynamic model for the North Atlantic, *Norw. J. Geol.*, 82, 281–298.
- Nieto-Samaniego, A. F., and S. A. Alaniz-Alvarez (1997), Origin and tectonic interpretation of multiple fault patterns, *Tectonophysics*, 270, 197–206.
- Oertel, G. (1965), The mechanics of faulting in clay experiments, *Tectonophysics*, 2, 343–393.
- Oldow, J. S. (2003), Active transensional boundary zone between the western Great Basin and the Sierra Nevada block, western U.S. Cordillera, *Geology*, 31, 1033–1036.
- Olesen, O., H. Henkel, K. Kaada, and E. Tveten (1991), Petrophysical properties of a prograde amphibolite-granulite facies transition zone at Sigerfjord, Vesterålen, northern Norway, *Tectonophysics*, 192, 33–39.
- Olesen, O., T. H. Torsvik, E. Tveten, K. B. Zwaan, T. Løseth, and T. Henningsen (1997), Basement structure of the continental margin in Lofoten-Lopphavet area, northern Norway: Constraints from potential field data, on-land structural mapping and palaeomagnetic data, *Nor. Geol. Tidsskr.*, 77, 15–30.
- Olesen, O., E. R. Lundin, O. Nordgulen, P. T. Osmundsen, J. R. Skilbrei, M. A. Smethurst, A. Solli, T. Bugge, and C. Fichler (2002), Bridging the gap between the onshore and offshore geology in Nordland, northern Norway, *Norw. J. Geol.*, 82, 243–262.
- Olesen, O., J. Ebbing, E. Lundin, J. R. Skilbrei, T. H. Torsvik, E. K. Hansen, T. Henningsen, P. Midbøe, and M. Sand (2005), A new tectonic model for the Eocene opening of the Norwegian-Greenland Sea - simplified geology by using modern aeromagnetic data, paper EGU05-A-02692 presented at the EGU 2nd General Assembly, Vienna, Austria, 24–29 April.
- Peacock, D. C. P., R. J. Knipe, and D. J. Sanderson (2000), Glossary of normal faults, *J. Struct. Geol.*, 22, 291–305.
- Petit, J. P. (1987), Criteria for the sense of movement on fault surfaces in brittle rocks, *J. Struct. Geol.*, 9, 597–608.
- Piazolo, S., G. I. Alsop, B. Møller Nielsen, and J. A. M. van Gool (2004), The application of GIS to unravel patterns of deformation in high grade terrains: A case study of indenter tectonics from west Greenland, in *Flow Processes in Faults and Shear Zones*, edited by G. I. Alsop et al., *Geol. Soc. Spec. Publ.*, 224, 63–78.
- Pollard, D. D., S. D. Saltzer, and A. M. Rubin (1993), Stress inversion methods: Are they based on faulty assumptions?, *J. Struct. Geol.*, 15, 1045–1054.
- Potts, G. J., and S. M. Reddy (1999), Construction and systematic assessment of relative deformation histories, *J. Struct. Geol.*, 21, 1245–1254.
- Ramsay, J. G., and R. J. Lisle (2000), *The Techniques of Modern Structural Geology*, vol. 3, *Applications of Continuum Mechanics in Structural Geology*, pp. 785–810, Elsevier, New York.

- Reches, Z. (1978), Analysis of faulting in a three-dimensional strain field, *Tectonophysics*, *47*, 109–129.
- Reches, Z. (1987), Determination of the tectonic stress tensor from slip along faults that obey the Coulomb yield condition, *Tectonics*, *6*, 849–861.
- Ren, S., J. I. Faleide, O. Eldholm, J. Skogseid, and F. Gradstein (2003), Late Cretaceous-Paleocene tectonic development of the NW Vøring Basin, *Mar. Pet. Geol.*, *20*, 177–206.
- Rosendahl, B. R. (1987), Architecture of continental rifts with special reference to East Africa, *Annu. Rev. Earth Planet. Sci.*, *15*, 445–503.
- Sagy, A., Z. Reches, and A. Agnon (2003), Hierarchic three-dimensional structure and slip partitioning in the western Dead Sea pull-apart, *Tectonics*, *22*(1), 1004, doi:10.1029/2001TC001323.
- Sanderson, D. J., and W. R. D. Marchini (1984), Transpression, *J. Struct. Geol.*, *6*, 449–458.
- Schreurs, G., and B. Colletta (1998), Analogue modeling of faulting in zones of continental transpression and transtension, in *Continental Transpressional and Transtensional Tectonics*, edited by R. E. Holdsworth, R. A. Strachan, and J. F. Dewey, *Geol. Soc. Spec. Publ.*, *135*, 59–79.
- Sellevoll, M. A. (1983), The study of the Earth in the island area of Lofoten-Vesterålen, northern Norway, *Norg. Geol. Undersøkelse*, *380*, 235–243.
- Sherlock, S. C. (2001), Two stage erosion and deposition in a continental margin setting: An $^{40}\text{Ar}/^{39}\text{Ar}$ laserprobe study of offshore detrital white micas in the Norwegian Sea, *J. Geol. Soc. London*, *158*, 793–799.
- Skogseid, J., T. Pedersen, O. Eldhom, and B. T. Larsen (1992), Tectonism and magmatism during NE Atlantic continental break-up, the Vøring margin, in *Magmatism and the Cause of Continental Break-up*, edited by B. C. Storey, T. Alabaster, and R. J. Pankhurst, *Geol. Soc. Spec. Publ.*, *68*, 305–320.
- Skogseid, J., S. Planke, J. I. Faleide, J. T. Pedersen, O. Eldhom, and F. Neverdal (2000), NE Atlantic continental rifting and volcanic margin formation in *Dynamics of the Norwegian Margin*, edited by A. Nottvedt, *Geol. Soc. Spec. Publ.*, *167*, 295–326.
- Smith, J. V., and D. W. Durney (1992), Experimental formation of brittle structural assemblages in oblique divergence, *Tectonophysics*, *216*, 235–253.
- Song, T., P. A. Cawood, and M. Middleton (2001), Transfer zones normal and oblique to rift trend: Examples from the Perth Basin, Western Australia, in *Non-volcanic Rifting of Continental Margins: A Comparison of Evidence for Land and Sea*, edited by R. C. L. Wilson et al., *Geol. Soc. Spec. Publ.*, *187*, 475–488.
- Steltenpohl, M. G., W. E. Hames, and A. Andresen (2004), The Silurian to Permian history of a metamorphic core complex in Lofoten, northern Scandinavian Caledonides, *Tectonics*, *23*, TC1002, doi:10.1029/2003TC001522.
- Strömberg, A. (1976), A pattern of tectonic zones in the western part of the East European Platform, *Geol. Foeren. Stockholm Foerh.*, *98*, 227–243.
- Talwani, M., and O. Eldholm (1977), Evolution of the Norwegian–Greenland Sea, *Geol. Soc. Am. Bull.*, *83*, 969–999.
- Taylor, B., K. Crook, and J. Sinton (1994), Extensional transform zones and oblique spreading centres, *J. Geophys. Res.*, *99*, 19,707–19,718.
- Teyssier, C., and B. Tikoff (1999), Fabric stability in oblique convergence and divergence, *J. Struct. Geol.*, *21*, 969–974.
- Thomson, K., and J. R. Underhill (1993), Development and evolution of structural styles in the Inner Moray Firth, in *Petroleum Geology of Northwest Europe: Proceedings of the 4th Conference*, edited by J. R. Parker, pp. 1167–1178, Geol. Soc., London.
- Titus, S. J., H. Fossen, R. B. Pedersen, J. L. Vigneresse, and B. Tikoff (2002), Pull-apart formation and strike-slip partitioning in an obliquely divergent setting, Leka Ophiolite, Norway, *Tectonophysics*, *354*, 101–119.
- Tsikalas, F., J. I. Faleide, and O. Eldholm (2001), Lateral variations in tectono-magmatic style along the Lofoten-Vesterålen volcanic margin off Norway, *Mar. Pet. Geol.*, *18*, 807–832.
- Tull, J. F., J. M. Bartley, K. V. Hodges, A. Andresen, M. G. Steltenpohl, and J. M. White (1985), The Caledonides in the Ofoten region (68–69N), north Norway: Key aspects of tectonic evolution, in *The Caledonian Orogen—Scandinavia and Related Areas*, edited by D. G. Gee and B. A. Sturt, pp. 553–569, John Wiley, Hoboken, N. J.
- Tveten, E. (1978), Geologisk kart over Norge, Berggrunnskart SVOLVÆR 1:250,000, Norw. Geol. Undersøkelse, Oslo.
- Tveten, E., and K. B. Zwaan (1993), Geology of the coast-region from Lofoten to Loppa, with special emphasis on faults, joints and related structures, *Norg. Geol. Undersøkelse Rep.*, *93.083*.
- Wilson, R. W., K. J. W. McCaffrey, R. E. Holdsworth, R. R. Jones, J. Imber, and P. Clegg (2005), Lofoten has its faults! Detailed fault analysis and 3D digital mapping in Norway's Lofoten Islands, *Geoscientist*, *15*(2), 1–9.
- Withjack, M. O., and W. R. Jamison (1986), Deformation produced by oblique rifting, *Tectonophysics*, *126*, 99–124.
- Xu, X., J. A. Battacharya, R. K. Davis, and C. L. V. Aiken (2000), Digital geological mapping of the Ferron Sandstone, Muddy Creek, Utah, with GPS and reflectorless laser rangefinders, *GPS Solutions*, *5*, 15–23.

R. E. Holdsworth, J. Imber, K. J. W. McCaffrey, and R. W. Wilson, Reactivation Research Group, Department of Earth Sciences, University of Durham, Durham DH1 3LE, UK. (r.e.holdsworth@durham.ac.uk; robert.wilson@durham.ac.uk)

R. R. Jones, Geospatial Research Ltd., Department of Earth Sciences, University of Durham, Durham DH1 3LE, UK.

D. Roberts, Geological Survey of Norway, N-7491 Trondheim, Norway.

A. I. F. Welbon, Statoil ASA, Forushagen, Grenseveien 21, N-4035 Stavanger, Norway.